ISSN 1948-5204 (online)

World Journal of *Gastrointestinal Oncology*

World J Gastrointest Oncol 2023 September 15; 15(9): 1505-1674

Published by Baishideng Publishing Group Inc

World Journal of Gastrointestinal Oncology

Contents

Monthly Volume 15 Number 9 September 15, 2023

World Journal of Gastrointestinal Oncology

Monthly Volume 15 Number 9 September 15, 2023

Contents

World Journal of Gastrointestinal Oncology

Monthly Volume 15 Number 9 September 15, 2023

Contents

NAME OF JOURNAL
World Journal of Gastrointestinal Oncology

ISSN
ISSN 1948-5204 (online)

LAUNCH DATE
February 15, 2009

FREQUENCY
Monthly

EDITORS-IN-CHIEF
Monjur Ahmed, Florin Burada

EDITORIAL BOARD MEMBERS
https://www.wjgnet.com/1948-5204/editorialboard.htm

PUBLICATION DATE
September 15, 2023

INSTRUCTIONS TO AUTHORS
https://www.wjgnet.com/bpg/gerinfo/204

GUIDELINES FOR ETHICS DOCUMENTS
https://www.wjgnet.com/bpg/GerInfo/287

GUIDELINES FOR NON-NATIVE SPEAKERS OF ENGLISH
https://www.wjgnet.com/bpg/gerinfo/240

PUBLICATION ETHICS
https://www.wjgnet.com/bpg/GerInfo/288

PUBLICATION MISCONDUCT
https://www.wjgnet.com/bpg/gerinfo/208

ARTICLE PROCESSING CHARGE
https://www.wjgnet.com/bpg/gerinfo/242

STEPS FOR SUBMITTING MANUSCRIPTS
https://www.wjgnet.com/bpg/GerInfo/239

ONLINE SUBMISSION
https://www.f6publishing.com

World Journal of Gastrointestinal Oncology

Submit a Manuscript: https://www.f6publishing.com

World J Gastrointest Oncol 2023 September 15; 15(9): 1567-1594

DOI: 10.4251/wjgo.v15.i9.1567

ISSN 1948-5204 (online)

ORIGINAL ARTICLE

Clinical and Translational Research

Cellular senescence throws new insights into patient classification and pharmacological interventions for clinical management of hepatocellular carcinoma

Hou-Hong Wang, Wen-Li Chen, Ya-Yun Cui, Hui-Hui Gong, Heng Li

Specialty type: Oncology

Provenance and peer review: Unsolicited article; Externally peer reviewed.

Peer-review model: Single blind

Peer-review report's scientific quality classification

Grade A (Excellent): 0
Grade B (Very good): 0
Grade C (Good): C, C
Grade D (Fair): 0
Grade E (Poor): 0

P-Reviewer: Nagaya M, Japan; Ozturk M, Turkey

Received: February 13, 2023
Peer-review started: February 13, 2023
First decision: May 23, 2023
Revised: July 10, 2023
Accepted: August 6, 2023
Article in press: August 6, 2023
Published online: September 15, 2023

Hou-Hong Wang, Wen-Li Chen, Department of General Surgery, The Affiliated Bozhou Hospital of Anhui Medical University, Bozhou 236800, Anhui Province, China

Ya-Yun Cui, Department of Cancer Radiotherapy, The First Affiliated Hospital of USTC, Division of Life Sciences and Medicine, University of Science and Technology of China (Anhui Provincial Cancer Hospital), Hefei 230000, Anhui Province, China

Hui-Hui Gong, Faculty of Health and Life Sciences, Oxford Brookes University, Oxford OX3 0BP, United Kingdom

Heng Li, Department of Comprehensive Surgery, Anhui Provincial Cancer Hospital, West District of The First Affiliated Hospital of USTC, Hefei 230000, Anhui Province, China

Corresponding author: Heng Li, Doctor, Professor, Department of Comprehensive Surgery, Anhui Provincial Cancer Hospital, West District of The First Affiliated Hospital of USTC, No. 17 Lujiang Road, Hefei 230000, Anhui Province, China. jxna36@163.com

Abstract

BACKGROUND

Cellular senescence, a state of stable growth arrest, is intertwined with human cancers. However, characterization of cellular senescence-associated phenotypes in hepatocellular carcinoma (HCC) remains unexplored.

AIM

To address this issue, we delineated cellular senescence landscape across HCC.

METHODS

We enrolled two HCC datasets, TCGA-LIHC and International Cancer Genome Consortium (ICGC). Unsupervised clustering was executed to probe tumor heterogeneity based upon cellular senescence genes. Least absolute shrinkage and selection operator algorithm were utilized to define a cellular senescence-relevant scoring system. *TRNP1* expression was measured in HCCs and normal tissues through immunohistochemistry, immunoblotting and quantitative real-time polymerase chain reaction. The influence of TMF-regulated nuclear protein (TRNP)1 on HCC senescence and growth was proven *via* a series of experiments.

RESULTS
TCGA-LIHC patients were classified as three cellular senescence subtypes, named C1–3. The robustness and reproducibility of these subtypes were proven in the ICGC cohort. C2 had the worst overall survival, C1 the next, and C3 the best. C2 presented the highest levels of immune checkpoints, abundance of immune cells, and immunogenetic indicators. Thus, C2 might possibly respond to immunotherapy. C2 had the lowest somatic mutation rate, while C1 presented the highest copy number variations. A cellular senescence-relevant gene signature was generated, which can predict patient survival, and chemo- or immunotherapeutic response. Experimentally, it was proven that TRNP1 presented the remarkable upregulation in HCCs. TRNP1 knockdown induced apoptosis and senescence of HCC cells and attenuated tumor growth.

CONCLUSION
These findings provide a systematic framework for assessing cellular senescence in HCC, which decode the tumor heterogeneity and tailor the pharmacological interventions to improve clinical management.

Key Words: Cellular senescence; Hepatocellular carcinoma; Prognosis; Subtypes; Tumor microenvironment; Gene signature; Pharmacological interventions

Core Tip: Cellular senescence, a state of stable growth arrest, is implicated in human cancers. Nevertheless, characterization of cellular senescence-associated phenotypes in hepatocellular carcinoma (HCC) is still indistinct. Here, we proposed a novel cellular senescence-based classification for HCC and identified TRNP1 as a novel therapeutic target.

Citation: Wang HH, Chen WL, Cui YY, Gong HH, Li H. Cellular senescence throws new insights into patient classification and pharmacological interventions for clinical management of hepatocellular carcinoma. *World J Gastrointest Oncol* 2023; 15(9): 1567-1594
URL: https://www.wjgnet.com/1948-5204/full/v15/i9/1567.htm
DOI: https://dx.doi.org/10.4251/wjgo.v15.i9.1567

INTRODUCTION

Cellular senescence is defined as an irreversible cessation of cellular division of cells with normal proliferation[1]. Human cells age due to progressive shortening of telomeres following cellular division, stress, oncogenes, *etc*[2]. Numerous genes have been implicated in cellular senescence as biomarkers and causal drivers[3,4]. Cellular senescence is a double-edged sword for cancer and its treatment[5,6]. The growth arrest and immunomodulatory features linked with senescence possess powerful antimalignant roles[7]. In addition, senescence bypass and secretory phenotype correlate to tumor progression and recurrence[8]. Research has unveiled the great potential for antiaging interventions as a novel antitumor strategy[9]. Nonetheless, the heterogeneity of senescence-related features makes the definition and targeting of treatment-induced senescent cells challenging[10].

Hepatocellular carcinoma (HCC) is a poorly managed malignancy with high mortality due to the lack of response to classical chemotherapy agents (doxorubicin, cisplatin, *etc*.) and targeted agents in the early stage[11]. For late-stage HCCs, single sorafenib or combination therapy remains the mainstay in first-line therapy, which improves overall survival by 3 mo[12]. The modest therapeutic success is largely attributable to sorafenib resistance[13]. Immunotherapy with checkpoint inhibitors (anti-PD-1/PD-L1) has displayed potent anti-HCC activity in a subset of patients[14]. The main unmet challenge in HCC immunotherapy is to discover and verify predictive biomarkers[15]. Accumulated evidence demonstrates that inducing tumor cells into senescence represents a potential anti-HCC therapy[16]. In HCCs, cellular senescence is primarily controlled by p53-dependent or -independent mechanisms[17]. Paradis *et al*[18] investigated replicative senescence in normal liver, chronic hepatitis C, and HCC, and demonstrated that chronic hepatitis C is a relevant model of accelerated replicative senescence and that accumulation of replicative senescent cells predispose to HCC progression[18]. Hepatic stellate cell activation and senescence also trigger the development of liver cirrhosis towards HCC[19]. Yildiz *et al*[20] found that cirrhosis and HCC exhibit expression patterns compatible with senescent and immortal phenotypes, respectively, while dysplasia is a transitional state. Senescence bypass exerts an essential role in hepatocellular carcinogenesis engendering systematic alteration in the transcription of genes modulating DNA repair, proliferation, differentiation, metabolism, *etc*[20]. Eggert *et al*[21] reported that while chemokines secreted by senescent hepatocytes inhibit liver cancer initiation, they enable to facilitate the growth of fully established HCC[21]. Due to the highly heterogeneous malignancy at the molecular and histological levels, characterization of cellular senescence-based classification might facilitate the personalized treatment of HCCs. Recently, cell senescence molecular subtypes have been conducted for predicting prognostic outcomes and immunotherapeutic responses of hepatitis B virus-related HCC patients[22]. A cellular-senescence-related classifier has been developed for inferring predicting prognosis, immunothera-

peutic responses, and candidate agents in HCCs[23]. However, these findings are based upon retrospective analysis, and lack of experimental validation. To address these problems, our integrative analysis classified HCCs as three cellular senescence subtypes and defined a cellular senescence-relevant scoring system, which decoded the tumor heterogeneity as well as tailored the pharmacological interventions to boost clinical management of HCC.

MATERIALS AND METHODS

Acquisition of cellular senescence genes

Totally, 279 human cellular senescence genes were acquired from the CellAge database (https://genomics.senescence.info/cells/)[3,4]. Genes that induce cellular senescence present the overexpression with age in human tissue samples and are notably overrepresented in antilongevity and tumor-suppressor genes; meanwhile, genes that inhibit cellular senescence overlap with prolongevity genes and oncogenes. The detailed information is listed in Supplementary Table 1.

Public HCC datasets

HCC patients were acquired from three public datasets, covering the Cancer Genome Atlas (TCGA-LIHC) database (https://portal.gdc.cancer.gov/projects/TCGA-LIHC) (n = 368), the International Cancer Genome Consortium (ICGC) portal (https://dcc.icgc.org/projects/LIRI-JP/) (n = 232), and the GSE14520 (https://www.ncbi.nlm.nih.gov/geo/query/acc.cgi?acc=GSE14520). Clinicopathological traits of above datasets are summarized in Supplementary Table 2. All expression data were transformed o transcripts per kilobase million, followed by log-2 conversion.

Differential expression analysis

Utilizing limma package, differentially expressed cellular senescence genes were screened in HCC relative to normal liver tissues[24]. To prevent high false-positive rate, P values were adjusted *via* Benjamini–Hochberg approach. Adjusted $P < 0.01$ and $|\log_2$ fold change (FC)$| > 0.58$ were regarded as the criteria of differentially expressed genes.

Functional annotation analysis

Gene Ontology (GO) and Kyoto Encyclopedia of Genes and Genomes (KEGG) were annotated by use of clusterProfiler package[25]. GO terms and KEGG pathways with adjusted $P < 0.05$ were significantly enriched. The activity of fifty hallmark pathways was computed through GSVA package[26] based upon the gene sets of Molecular Signatures Database[27].

Unsupervised clustering

Based upon the prognostic differentially expressed cellular senescence genes derived from univariate Cox regression ($P < 0.05$), unsupervised clustering was implemented for TCGA-LIHC patients utilizing ConsensusClusterPlus package[28]. This process was conducted with 1000 iterations through sampling 80% of all the data for each iteration, thus ensuring clustering stability. The optimal number of clusters was identified utilizing consensus heatmap together with cumulative distribution function (CDF) curves. Principal component analysis (PCA) was utilized for recognizing and visualizing distinct subtypes.

Nearest template prediction for subtype verification

Nearest template prediction (NTP) method is flexible for evaluating class prediction confidence for patients. Up-regulated genes were regarded as markers of each subtype with adjusted $P < 0.05$, which were adopted in the NTP method derived from CMScaller package[29], thus assessing the reliability and stability of subtypes.

Tumor microenvironment estimation

Single-cell gene set enrichment analysis (ssGSEA), a deconvolution algorithm from GSVA package, was executed for quantifying the compositions within the tumor microenvironment (TME), comprising 22 immune cells and two stromal components (fibroblasts and endothelial cells). The ssGSEA score denoted the abundance of these TME components. The abundance of the TME components was also inferred through TIMER, CIBERSORT, CIBERSORT-ABS, QUANTISEQ, MCPCOUNTER, XCELL, together with EPIC methods.

Genetic alteration analysis

The available mutation annotation format files from the TCGA were adopted for the analysis of somatic mutation utilizing maftools package[30]. Copy number variations (CNVs) of TCGA HCCs were stratified into three cellular senescence subtypes. Significant amplifications or deletions across the whole genome were assessed utilizing GISTIC2.0 [31].

Cellular senescence subtype-relevant gene selection

Genes with differential expression between subtypes were selected with the thresholds of adjusted $P < 0.05$ together with $|\log_2 FC| > 0.58$. Cellular senescence subtype-relevant genes were determined following the intersection.

Gene signature establishment

Univariate Cox regression analysis was utilized for picking out cellular-senescence-relevant genes with prognostic implication based upon $P < 0.05$. Through least absolute shrinkage and selection operator (LASSO) algorithm, the best gene subset was found out *via* glmnet package[32]. The cellular senescence-relevant scoring system was defined following the formula: RiskScore = Σ(coefficient (β)*Expression β), where β denoted each selected prognostic cellular senescence-relevant gene. HCCs were stratified into low- and high-RiskScore groups with the median RiskScore.

Nomogram construction

Uni- and multivariate Cox regression analyses on the cellular-senescence-relevant gene signature and conventional clinicopathological variables were executed to select independent prognostic factors in the TCGA-LIHC cohort. A nomogram based upon independent factors was generated to predict the probability of overall survival through rms package. Decision curve analysis was conducted for validating the nomogram[33].

Therapeutic response prediction

The half-maximal inhibitory concentration (IC_{50}) value of commonly used chemotherapy or targeted therapy drugs was inferred utilizing pRRophetic package[34]. Immunotherapy response was inferred by use of Tumor Immune Dysfunction and Exclusion (TIDE)[35].

Patients and tissues

Thirty fresh HCC tumors together with adjacent normal tissues were harvested from The Affiliated Bozhou Hospital of Anhui Medical University. No patients experienced any preoperative adjuvant treatment. HCC diagnosis was confirmed pathologically. Written informed consent was provided by each patient. This project gained the approval of the Ethics Committee of The Affiliated Bozhou Hospital of Anhui Medical University (2022-17).

Immunohistochemistry

TRNP1 expression in HCC or normal tissues was tested through fixing tissue sections with 4% paraformaldehyde. The sections were sealed utilizing goat serum, followed by incubation with TRNP1 antibody (1:500; ab174303; Abcam, Cambridge, MA, USA) along with secondary antibody (1/1000; ab7090). After administration with diaminobenzidine tetrahydrochloride, images were acquired under a microscope (Zeiss, Germany).

Immunoblotting

Total protein extraction was analyzed utilizing immunoblotting. Protein content was measured utilizing BCA kit (Beyotime, Shanghai, China). Proteins were separated *via* 12% SDS-PAGE, and transferred onto PVDF membranes that were then probed with primary antibody against TRNP1 (1/5000; ab174303; Abcam), p16 (1/500; ab151303), p21 (1/1000; ab109199) or GAPDH (1/2500; ab9485) at 4°C overnight, and secondary antibody (1/1000; ab7090) at room temperature for 2 h. Proteins were developed using ECL reagent (Beyotime).

Quantitative real-time polymerase chain reaction

RNA extraction was achieved utilizing RNA easy mini kit (Invitrogen, Carlsbad, CA, USA), with cDNA preparation *via* PrimeScript RT Master Mix (Takara, Dalian, China). Quantitative real-time polymerase chain reaction (RT-qPCR) was conducted *via* ChamQ SYBR qPCR Master Mix (Vazyme, Nanjing, China). The relative expression value was estimated with $2^{-\Delta\Delta Ct}$ approach as well as normalized to endogenous GAPDH.

Cell culture and transfection

RPMI-1640 medium (Gibco) containing 10% fetal bovine serum (Gibco), and 1% penicillin–streptomycin (Gibco) was adopted for culturing SMMC-7721 and HepG2 HCC cells. All cells were maintained in an incubator at 37°C with 5% CO_2. For transfection, siRNAs of TRNP1 (si-TRNP1) and negative control (si-NC) were acquired from GenePharma. Cell transfection was conducted utilizing Lipofectamine 2000 (Thermo Fisher Scientific).

Flow cytometry

Apoptotic rate was tested through flow cytometry utilizing Annexin V–fluorescein isothiocyanate (apoptosis detection kit (BD Biosciences). Cells were harvested and the assay was performed. Next, samples were assessed instantly utilizing flow cytometry (Beckman Coulter).

SA-β-galactosidase staining

To investigate senescence, 10^4 cells were seeded onto a six-well plate. After being fixed, they were stained with senescence-associated -galactosidase activity (SA-β-gal) (Gibco).

Tumor xenograft

Female BALB/c nude mice (5-wk-old, 16–18 g; Beijing Vital River Laboratory Animal Technology Co. Ltd., China) were fed under a 12-h light/dark cycle. They were divided into three groups ($n = 5$ per group). SMMC-7721 cells ($n = 10^5$) with si-NC, si-TRNP1#1 or si-TRNP1#2 were inoculated into the armpit. After 36 d, they were killed, with subsequent tumor excision. Tumor volume was finally calculated. This experiment gained the approval the Animal Ethics Committee of The Affiliated Bozhou Hospital of Anhui Medical University (LLSC20232071).

Statistical analysis

For between-group comparisons, unpaired Student's *t*-test was adopted; Mann–Whitney *U* test was utilized for variables with non-normal distribution. Kaplan–Meier curves were utilized to estimate the overall survival of groups, with log-rank for testing the difference significance between groups. Survival analysis was executed utilizing survival and survminer packages. Receiver operator characteristic curves were plotted to evaluate the prediction efficacy in overall survival. Statistical analyses were implemented utilizing R packages and GraphPad Prism software. A two-sided $P < 0.05$ indicated statistical significance.

RESULTS

Differentially expressed cellular senescence genes in HCC and biological significance

We identified 146 differentially expressed cellular senescence genes in TCGA HCCs relative to normal tissues with adjusted $P < 0.01$ and $|\log_2 FC| > 0.58$ (Figure 1A and B; Supplementary Table 3), which might participate in HCC initiation or progression. They were linked with metabolic process, cellular senescence, cell cycle, and immunity pathways (Figure 1C–F). Their prognostic value was then assessed. Ninety-seven differentially expressed cellular senescence genes were significantly linked with HCC prognosis (Table 1).

Classification of HCC patients as three cellular senescence subtypes

Prognostic differentially expressed cellular senescence genes were utilized for probing HCC heterogeneity. Utilizing unsupervised clustering, TCGA-LIHC cases were initially assigned to 2–9 clusters. Combining consensus CDF and consensus matrix, the optimal number of clusters was generated when k = 3 (Figure 2A–C). Thus, HCCs were classified as three cellular senescence subtypes, named C1–3. Prognostic differentially expressed cellular senescence genes presented the highest transcript levels in C2, followed by C1 and C3 (Figure 2D). PCA proved the extensive discrepancy in transcript levels among three subtypes (Figure 2E). Additionally, we focused on the survival difference, with C2 having the worst overall survival, C1 the next, and C3 the best (Figure 2F). Based upon up-regulated markers of each subtype (Supplementary Table 4), the robustness and reproducibility of cellular senescence subtypes were verified utilizing NTP in the ICGC cohort (Figure 2G). The discrepancy in transcript levels and overall survival among subtypes was further proven in this cohort (Figure 2H and I).

Responses to immunotherapy and chemotherapy of three cellular senescence subtypes

To elucidate the underlying mechanisms among the three cellular senescence subtypes, the activity of 50 hallmark pathways was inferred. Tumorigenic pathways (DNA repair, MYC, PI3K–AKT–mTOR, mTORC1, *etc*.) exhibited the highest activity in C2, with the lowest activity of metabolism pathways (Figure 3A). C3 presented the lowest activity of tumorigenic pathways, as well as the highest activity of metabolism pathways. Additionally, it was found that immune checkpoints displayed the highest transcript levels in C2, with the highest abundance of immune cells (Figure 3B). Immunogenetic indicators were then observed. Aneuploidy score, cancer-testicular antigen score, homologous recombination defects, and intratumor heterogeneity displayed the highest levels in C2, followed by C1 and C3 (Figure 3C–F). TIDE score was utilized to estimate the response to immune checkpoint inhibitors. Among three subtypes, C3 presented the lowest TIDE score, indicating that this subtype was most likely to respond to immune checkpoint inhibitors (Figure 3G). It was also found that cisplatin, doxorubicin and gemcitabine showed the lowest IC_{50} values in C2 subtype (Figure 3H–J). Thus, C2 patients were most likely to benefit from above chemotherapeutic drugs.

Genetic alterations of three cellular senescence subtypes

Overall, somatic mutation rate was the lowest in C2 among three cellular senescence subtypes (Figure 4A–C). Additionally, C1 presented the highest copy number amplified and deleted alterations (Figure 4D–I). Altogether, there was remarkable heterogeneity in genetic alterations among three cellular senescence subtypes.

Identification of cellular senescence subtype-relevant genes and functional implications

To select cellular senescence subtype-relevant genes, we assessed the genes with differential expression between cellular senescence subtypes based upon adjusted $P < 0.05$ together with $|\log_2 FC| > 0.58$. After the intersection, 666 cellular senescence subtype-relevant genes were eventually acquired (Supplementary Table 5 and Figure 5A). We elucidated the underlying functional implications. Consequently, these cellular senescence subtype-relevant genes were remarkably linked with cell cycle, DNA replication, oocyte meiosis, homologous recombination, cellular senescence, Fanconi anemia pathway, p53 pathway, progesterone-mediated oocyte maturation, mismatch repair, *etc* (Figure 5B–E).

Definition and external verification of a cellular-senescence-relevant gene signature

To illustrate the relationships of the cellular-senescence-relevant genes and patient survival, univariate Cox regression method was adopted. A total of 511 cellular -enescence-relevant genes presented significant correlations to TCGA-LIHC prognosis (Supplementary Table 6). These prognostic genes were entered into LASSO analysis (Figure 6A and B). A 19-gene signature was generated in accordance with the optimal λ value. The cellular senescence-relevant scoring system was computed as follows: RiskScore = 0.0610156 * transcript level of SLC1A5 + 0.049731458 * transcript level of G6PD + 0.038762092 * transcript level of PSRC1 + 0.104396819 * transcript level of UCK2 + 0.004054037 * transcript level of TCOF1 + 0.03040522 * transcript level of CCT5 + 0.002669582 * transcript level of DTYMK + 0.053080689 * transcript level of

Table 1 Univariate-cox regression results of prognostic differentially expressed cellular senescence genes with *P* < 0.05 in TCGA-LIHC dataset

Gene	HR	95%lower	95%upper	*P* value	Gene	HR	95%lower	95%upper	*P* value
MCRS1	1.6954	1.2504	2.2988	0.0007	*TPR*	1.2593	1.0274	1.5436	0.0264
FASTK	1.3714	1.0147	1.8536	0.0399	*HDAC1*	1.8639	1.4442	2.4055	< 0.0001
AURKA	1.2794	1.1083	1.4770	0.0008	*SPOP*	1.4186	1.0061	2.0004	0.0461
PTTG1	1.3361	1.1782	1.5151	< 0.0001	*BTG3*	1.3304	1.0766	1.6440	0.0082
PSMB5	1.8929	1.3286	2.6969	0.0004	*IRF5*	1.4232	1.1118	1.8217	0.0051
MAP2K2	1.5424	1.1846	2.0083	0.0013	*IGFBP3*	1.1741	1.0435	1.3210	0.0076
E2F1	1.2175	1.0804	1.3721	0.0012	*CDKN2B*	1.3951	1.1619	1.6751	0.0004
CDK1	1.3097	1.1553	1.4847	< 0.0001	*AAK1*	1.3018	1.0160	1.6682	0.0371
GRK6	1.7940	1.3455	2.3920	< 0.0001	*ARPC1B*	1.3007	1.0918	1.5495	0.0032
EZH2	1.5722	1.3117	1.8845	< 0.0001	*LIMK1*	1.3450	1.1517	1.5706	0.0002
DPY30	1.9266	1.3785	2.6928	0.0001	*SFN*	1.1541	1.0714	1.2432	0.0002
CBX8	1.4643	1.1477	1.8684	0.0022	*CSNK2A1*	1.3825	1.0896	1.7541	0.0077
SMARCA4	1.4396	1.1405	1.8170	0.0022	*GLB1*	1.4265	1.1097	1.8336	0.0056
CDKN2A	1.1748	1.0571	1.3055	0.0028	*MOB3A*	1.4527	1.1459	1.8416	0.0020
IRF3	1.4048	1.0834	1.8216	0.0103	*BRD7*	1.3897	1.0401	1.8567	0.0260
HRAS	1.4678	1.1958	1.8016	0.0002	*PRKCD*	1.4989	1.2458	1.8035	< 0.0001
ADCK5	1.3095	1.0375	1.6527	0.0232	*CDK4*	1.4798	1.2301	1.7800	< 0.0001
RUVBL2	1.7508	1.3029	2.3528	0.0002	*BLVRA*	1.1790	1.0296	1.3500	0.0172
ACLY	1.3734	1.1160	1.6901	0.0027	*SENP1*	1.5189	1.1628	1.9840	0.0022
TACC3	1.3618	1.1752	1.5780	< 0.0001	*BMI1*	1.6112	1.2516	2.0742	0.0002
SIRT6	1.6515	1.2586	2.1671	0.0003	*DHX9*	1.3908	1.1069	1.7477	0.0046
SUPT5H	1.5227	1.1449	2.0252	0.0039	*RSL1D1*	1.7134	1.2421	2.3634	0.0010
FOXM1	1.2772	1.1287	1.4454	0.0001	*PAK4*	1.2908	1.0419	1.5990	0.0195
PSMD14	1.9715	1.5043	2.5838	< 0.0001	*PDCD10*	1.6080	1.2369	2.0903	0.0004
HJURP	1.4529	1.2514	1.6869	< 0.0001	*ASF1A*	1.7774	1.3749	2.2977	< 0.0001
TRIM28	1.6005	1.2816	1.9988	< 0.0001	*PNPT1*	1.6790	1.2487	2.2576	0.0006
P3H1	1.9307	1.5257	2.4431	< 0.0001	*MAPK12*	1.2163	1.0478	1.4119	0.0101
MAGOHB	1.4601	1.0477	2.0346	0.0254	*UBTD1*	1.3794	1.0584	1.7977	0.0173
RBX1	1.6692	1.2410	2.2451	0.0007	*KDM5B*	1.3241	1.1029	1.5895	0.0026
MAGOH	1.6449	1.1977	2.2592	0.0021	*USP1*	1.4478	1.1790	1.7778	0.0004
CENPA	1.4947	1.2958	1.7241	< 0.0001	*MAP3K7*	1.4740	1.1327	1.9180	0.0039
EWSR1	1.9373	1.3937	2.693	< 0.0001	*PKM*	1.2079	1.0979	1.3290	0.0001
HSPA5	1.3234	1.0428	1.6796	0.0212	*NINJ1*	1.4743	1.0929	1.9888	0.0110
CHEK1	1.5484	1.2766	1.8780	< 0.0001	*SERPINE1*	1.1201	1.0226	1.2269	0.0147
PIAS4	1.4493	1.0683	1.9663	0.0171	*BRCA1*	1.4378	1.1653	1.7741	0.0007
PRPF19	2.5587	1.7707	3.6974	< 0.0001	*DEK*	1.2103	1.0125	1.4468	0.0360
MAPKAPK5	2.0718	1.4388	2.9834	< 0.0001	*NDRG1*	1.2946	1.1412	1.4686	< 0.0001
MAD2L1	1.4390	1.2065	1.7164	< 0.0001	*SRC*	1.2011	1.0507	1.3730	0.0073
TFAP4	1.9651	1.4205	2.7184	< 0.0001	*ASPH*	1.2007	1.0488	1.3746	0.0081
G6PD	1.3897	1.2500	1.5450	< 0.0001	*STK32C*	1.5149	1.2235	1.8759	0.0001

GAPDH	1.5984	1.2892	1.9818	< 0.0001	*CDK2AP1*	1.2327	1.0010	1.5181	0.0490
SMARCB1	1.4393	1.1297	1.8336	0.0032	*KDM4A*	1.3363	1.0476	1.7045	0.0196
LEO1	1.4005	1.0359	1.8934	0.0286	*MMP9*	1.1360	1.0384	1.2428	0.0054
TXN	1.3040	1.0667	1.5941	0.0096	*HK3*	1.2356	1.0293	1.4832	0.0232
HDAC4	1.5029	1.1470	1.9692	0.0031	*VEGFA*	1.2906	1.0657	1.5630	0.0090
FXR1	1.6935	1.2509	2.2927	0.0007	*LGALS3*	1.2041	1.0826	1.3392	0.0006
RAD21	1.3480	1.0928	1.6629	0.0053	*AR*	0.8662	0.7749	0.9682	0.0115
SRSF1	1.7610	1.2427	2.4955	0.0015	*BAG3*	1.2740	1.0326	1.5718	0.0238

NEIL3 + 0.031271078 * transcript level of TRNP1 + (-0.037524429) * transcript level of ADH4 + 0.018409162 * transcript level of HMMR + 0.001793118 * transcript level of SMG5 + (-0.016621762) * transcript level of CLEC3B + 0.083327624 * transcript level of PLOD2 + 0.035535231 * transcript level of SPP1 + (-0.023169364) * transcript level of CFHR3 + 0.020042596 * transcript level of TMEM106C + (-0.019959706) * transcript level of ANXA10 + (-0.039577478) * transcript level of LCAT. Based upon the median RiskScore, TCGA-LIHC cases were classified as low- and high-RiskScore groups (Figure 6C). Expression levels of these selected genes exhibited the notable differences between groups. Next, K-M curves illustrated that high-RiskScore patients' overall survival was worse (Figure 6D). AUCs at 1-, 3- and 5-year survival all exceeded 0.75, demonstrating the excellent discrimination power of the gene signature (Figure 6E).

The ICGC and GSE14520 datasets were utilized to externally verify this signature. The current study stratified HCCs into low- and high-RiskScore groups based upon the median RiskScore in the ICGC dataset (Figure 6F). Overall survival rate of high-RiskScore group was prominently lower (Figure 6G). AUCs at 1- and 3-year survival were > 0.75 (Figure 6H). Above data proved the high reproducibility of the signature. The similar findings were also confirmed in the GSE14520 dataset (Figure 6I–K).

Generation of a prognostic nomogram for clinical practice

Univariate and multivariate Cox regression analyses were executed to select the independent prognostic parameters for HCCs. It was found that stage and the cellular-senescence-relevant RiskScore acted as independent risk factors of HCC prognosis (Figure 7A and B). As a visual representation of the prognostic model, a nomogram containing stage, and RiskScore was built to illustrate HCC patients' survival more intuitively. The nomogram showed that RiskScore had the highest influence on 1-, 3- and 5-year survival of HCC patients, followed by stage (Figure 7C). Decision curve analysis demonstrated that the nomogram can accurately predict 1-, 3- and 5-year clinical outcomes (Figure 7D–F).

Assessment of the cellular-senescence-relevant gene signature in predicting efficacy of pharmacological interventions

The IC_{50} of some chemotherapy or targeted therapy agents was estimated in TCGA-LIHC dataset. High-RiskScore HCCs presented the notably lower IC_{50} of cisplatin, doxorubicin, and gemcitabine relative to those with low RiskScore (Figure 8A–C). However, no significant difference in the IC_{50} of sorafenib was found between the two groups (Figure 8D). Accordingly, high-RiskScore HCCs more possibly responded to cisplatin, doxorubicin or gemcitabine chemotherapy.

Some reliable computational approaches were adopted to infer the abundance of the TME elements across TCGA-LIHC samples. Overall, most immune cells exhibited the higher infiltration in high-risk HCCs (Figure 8E). The TIDE method was used to predict immunotherapy response. We did not observe any difference in carcinoma-associated fibroblasts between the groups (Figure 8F). Lower myeloid-derived suppressor cells, interferon gamma, exclusion score and TIDE score as well as higher dysfunction score were found in low-RiskScore HCCs (Figure 8G–K). This indicated that low-RiskScore HCCs more possibly benefited from immunotherapy.

Experimental verification of expression of TRNP1 in HCC

Among the genes in the cellular-senescence-relevant gene signature, the role of TRNP1 in HCC remains unclear. Therefore, we focused on TRNP1. It was proven that TRNP1 presented remarkable upregulation in HCCs relative to normal tissues in accordance with immunohistochemistry (Figure 9A and B), immunoblotting (Figure 9C and D) and RT-qPCR (Figure E). Specific siRNAs of TRNP1 were transfected into SMMC-7721 and HepG2 cells. Immunoblotting demonstrated the notable decrease in TRNP1 expression induced by siRNAs (Figure 9F–9H).

Suppression of TRNP1 induces apoptosis and senescence of HCC cells and attenuates tumor growth

Based upon flow cytometry, apoptotic rate of SMMC-7721 and HepG2 cells was prominently elevated by TRNP1 knockdown (Figure 10A–C). SA-β-Gal staining showed that TRNP1 knockdown notably induced cellular senescence of two HCC cells (Figure 10D–F). Additionally, two cellular senescence markers: p16 and p21 were overexpressed in HCC cells with TRNP1 knockdown (Figure 10G–K), further proving the role of TRNP1 in HCC senescence. *In vivo* tumorigenicity models were also developed for evaluating whether TRNP1 influenced tumor growth. As a result, TRNP1 knockdown was found to decrease *in vivo* tumor volume (Figure 10L and M).

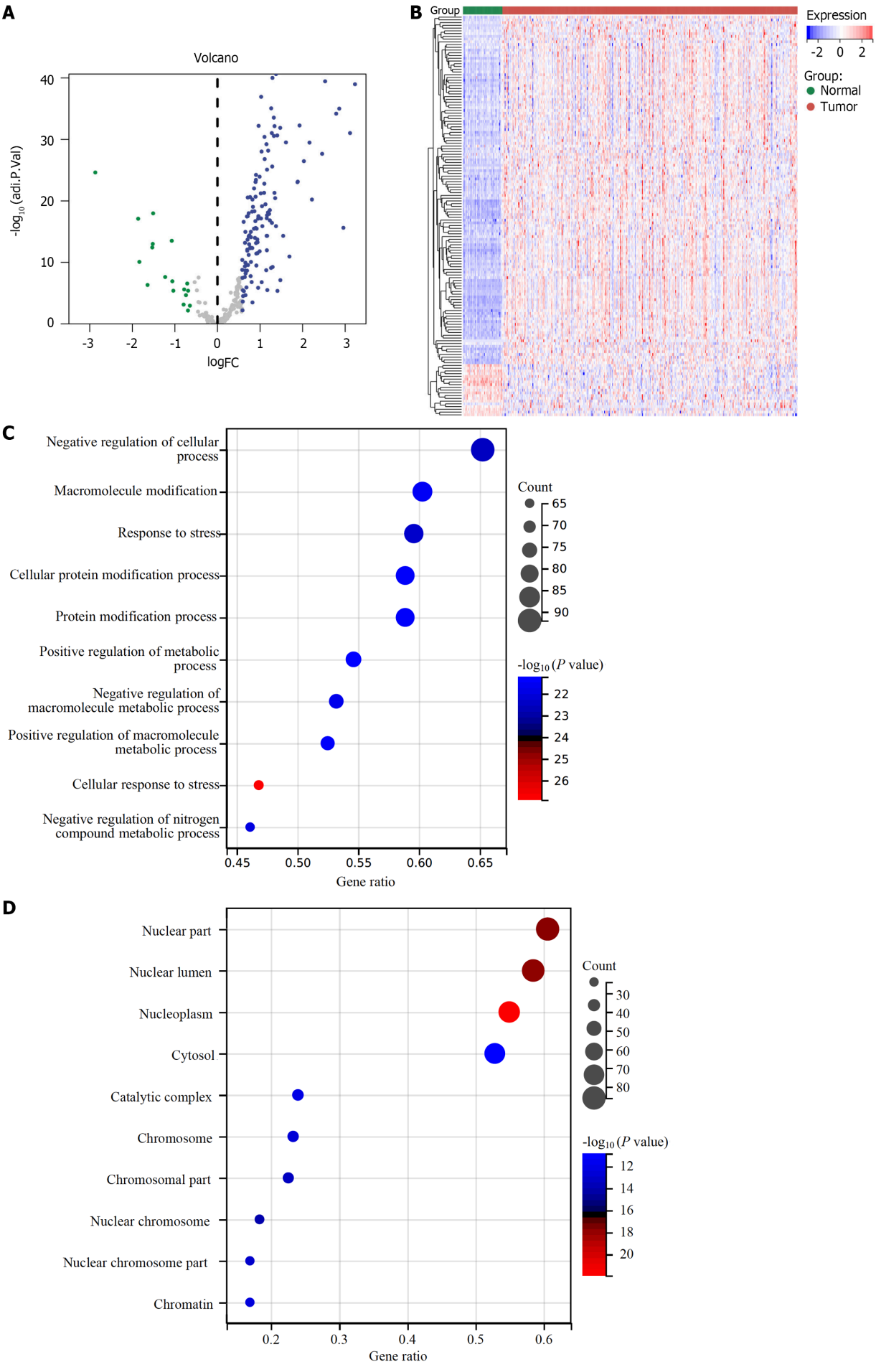
A
Volcano
-log10 (adj.P.Val)
logFC
B
Group
Expression
Group:
Normal
Tumor
C
Negative regulation of cellular process
Macromolecule modification
Response to stress
Cellular protein modification process
Protein modification process
Positive regulation of metabolic process
Negative regulation of macromolecule metabolic process
Positive regulation of macromolecule metabolic process
Cellular response to stress
Negative regulation of nitrogen compound metabolic process
Count
-log10 (P value)
Gene ratio
D
Nuclear part
Nuclear lumen
Nucleoplasm
Cytosol
Catalytic complex
Chromosome
Chromosomal part
Nuclear chromosome
Nuclear chromosome part
Chromatin
Count
-log10 (P value)
Gene ratio

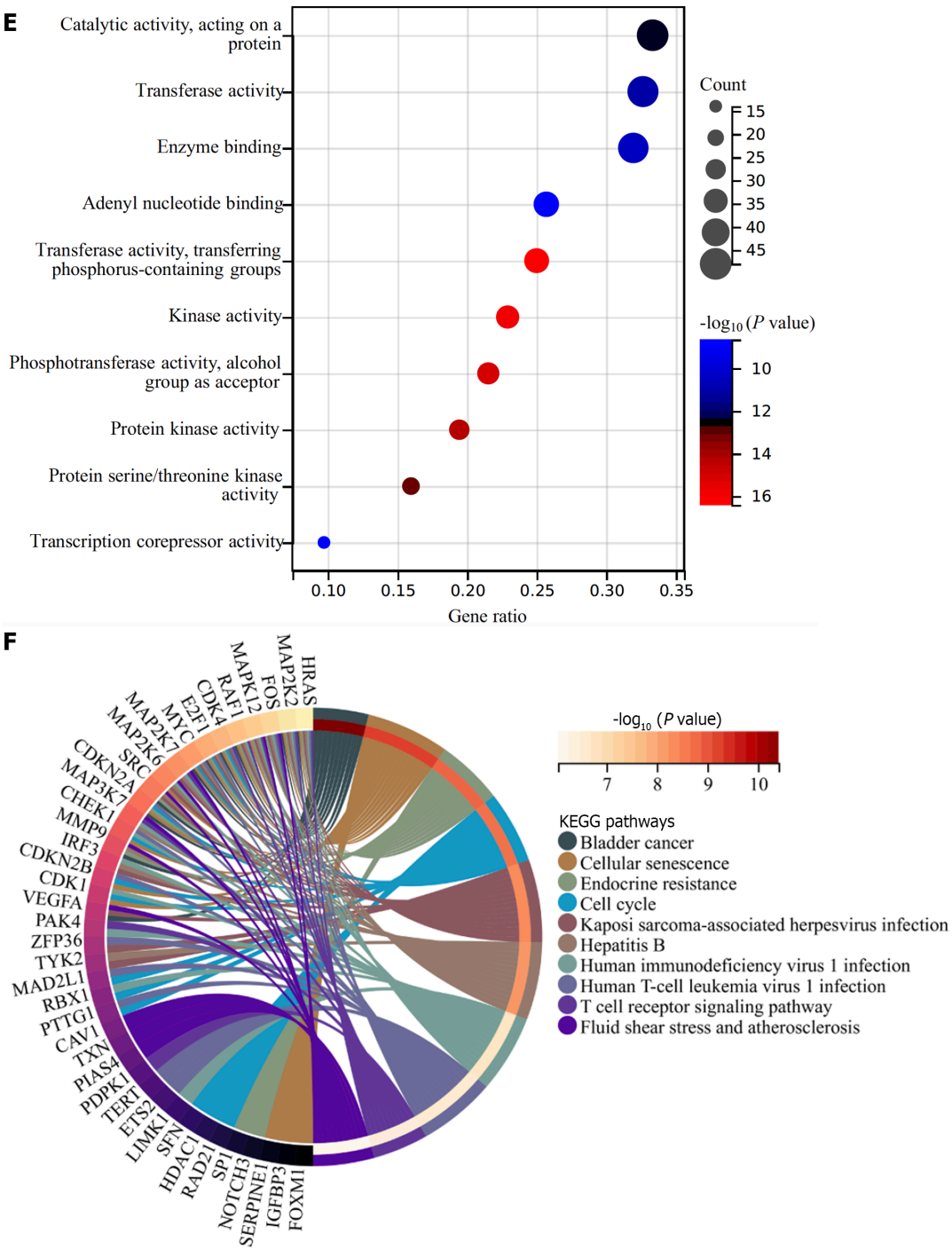

Figure 1 Differentially expressed cellular senescence genes in hepatocellular carcinoma and biological significance. A: Volcano diagram of the abnormal expression of cellular senescence genes in hepatocellular carcinoma (HCC) relative to normal liver tissues in the TCGA-LIHC dataset. Blue dots denote differentially expressed cellular senescence genes, with grey dots for the not differentially expressed genes; B: Heatmap of the transcript levels of differentially expressed cellular senescence genes in HCC and normal liver tissues; C–E: Bubble diagrams of the top 10 biological process, cellular component, molecular function terms enriched by differentially expressed genes. The bubble size indicates the count of genes enriched. The closer the color is to red, the smaller the adjusted p; F: Circle graph of the Kyoto Encyclopedia of Genes and Genomes pathways enriched by differentially expressed genes.

DISCUSSION

Cellular senescence is a permanent state of cell cycle arrest occurring in proliferating cells when face distinct stresses[36]. In cancers, senescence is usually an effective barrier against tumorigenesis because it prevents the division potential of cells[37]. Nonetheless, numerous research has demonstrated that senescent cells also have tumorigenic properties[38]. Thus, it is of significance to characterize key features of cellular senescence in HCC.

HCC is a typically fatal malignant tumor displaying genetic heterogeneity and limited therapy responses[39]. Based upon prognostic differentially expressed cellular senescence genes, we classified HCCs as three cellular senescence subtypes: C1–C3. The robustness and reproducibility of this classification were externally proven. C2 had the worst

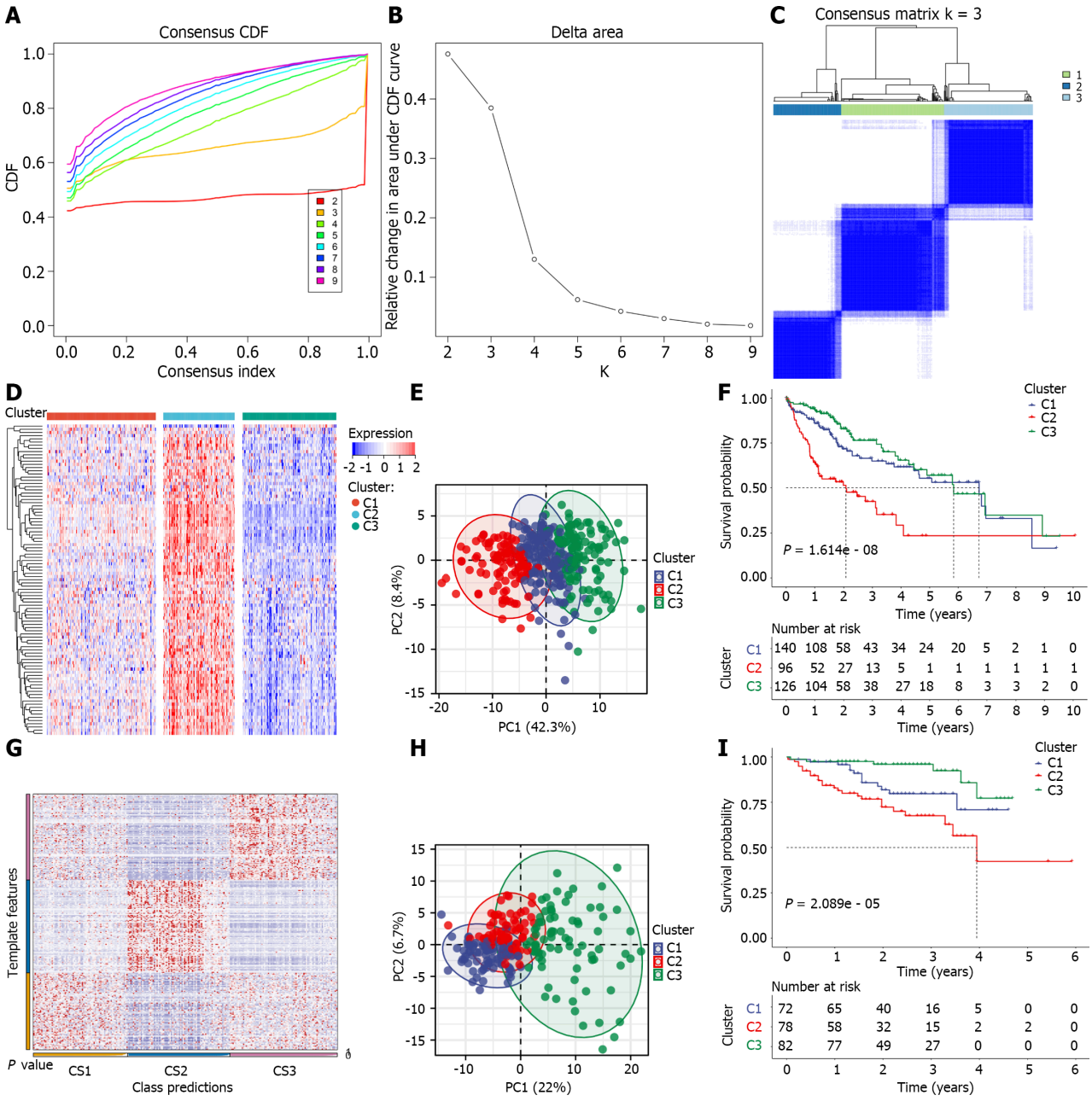

Figure 2 Classification of TCGA-LIHC patients as three cellular senescence subtypes and external dataset validation. A–C: Consensus cumulative distribution function (CDF), relative alteration in area under CDF curve, and consensus matrix k = 3 based upon the transcriptome of prognostic differentially expressed cellular senescence genes across TCGA-LIHC patients; D: The transcript levels of differentially expressed cellular senescence genes with prognostic implications across three subtypes; E: Principal component analysis (PCA) plots of the discrepancy in transcript levels among subtypes; F: Kaplan–Meier (K-M) curves of overall survival in TCGA-LIHC; G: Nearest template prediction for verifying the subtypes in the International Cancer Genome Consortium (ICGC) cohort; H and I: PCA plots of the transcriptome difference and K-M curves of overall survival among subtypes in the ICGC cohort.

overall survival, C1 the next, and C3 the best, revealing the heterogeneity in prognostic outcomes among subtypes. Single-agent anti-PD-1 immune checkpoint blockade showed ponent efficacy in early-phase trials, but the findings were not confirmed in phase III studies[40]. In accordance with the lowest TIDE score, and immunogenetic indicators, C3 HCCs might possibly respond to immunotherapy. Additionally, C2 HCCs were most likely to benefit from chemotherapy. Thus, this classification might assist clinical decision-making. Genetic mutations associate with HCC initiation and progression[41-43]. For instance, mutant TP53 is the most frequent in HCC, affecting patient survival, and immune response[44]. CTNNB1 mutation occupies a large proportion of human HCCs, which correlates to high TMB and AFP in HCCs[45]. Among three cellular senescence subtypes, C2 presented the lowest somatic mutation rate, while C1 had the highest frequent CNVs. Accordingly, cellular senescence subtypes appear to associate with genetic mutations.

We defined a novel cellular-senescence-relevant gene signature comprising SLC1A5, G6PD, PSRC1, UCK2, TCOF1, CCT5, DTYMK, NEIL3, TRNP1, ADH4, HMMR, SMG5, CLEC3B, PLOD2, SPP1, CFHR3, TMEM106C, ANXA10, and LCAT, with the excellent power in survival prediction in HCCs. Previous research has proven the biological implications of the cellular-senescence-relevant genes in HCC. For example, SLC1A5 regulated by DDR1 contributes to HCC

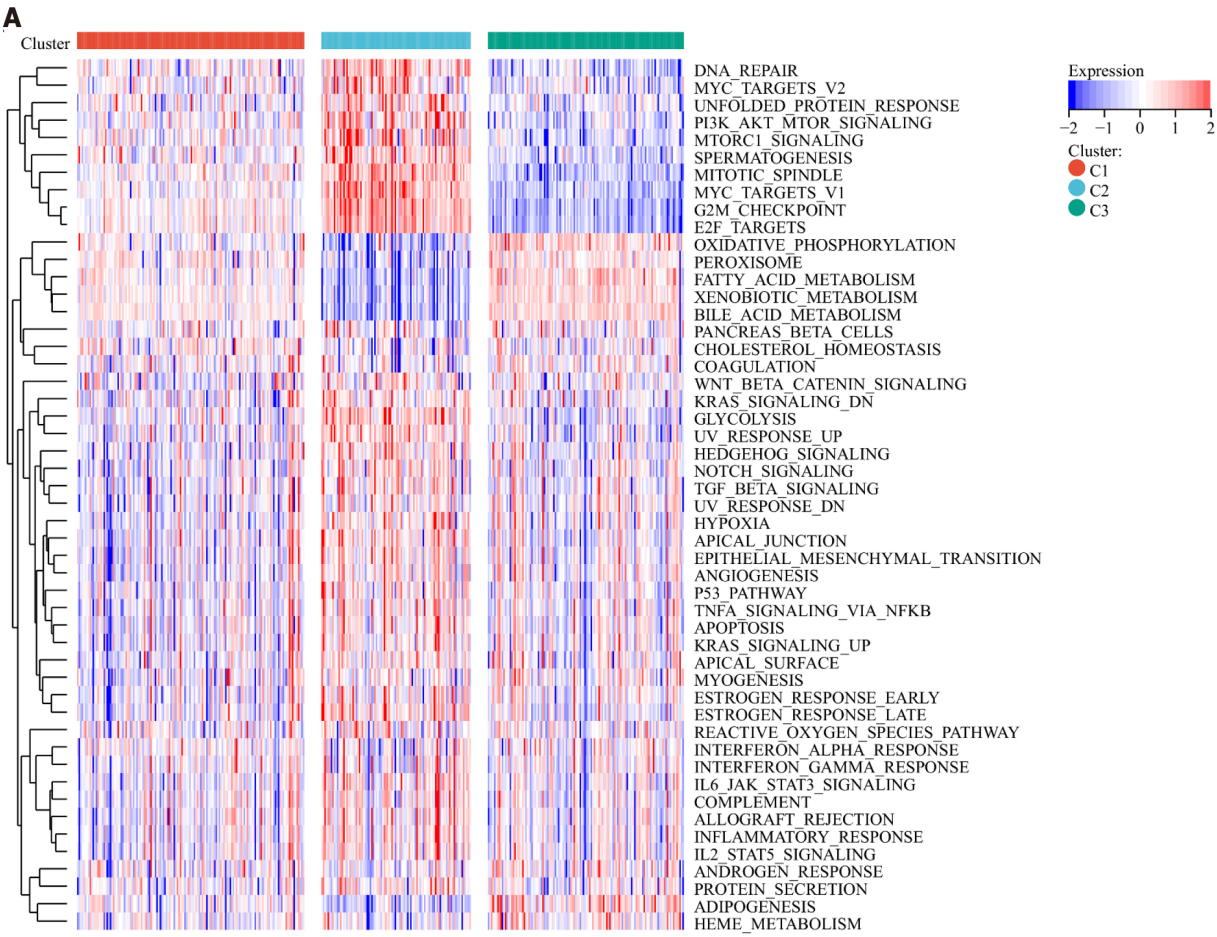
A
Cluster
DNA_REPAIR
MYC_TARGETS_V2
UNFOLDED_PROTEIN_RESPONSE
PI3K_AKT_MTOR_SIGNALING
MTORC1_SIGNALING
SPERMATOGENESIS
MITOTIC_SPINDLE
MYC_TARGETS_V1
G2M_CHECKPOINT
E2F_TARGETS
OXIDATIVE_PHOSPHORYLATION
PEROXISOME
FATTY_ACID_METABOLISM
XENOBIOTIC_METABOLISM
BILE_ACID_METABOLISM
PANCREAS_BETA_CELLS
CHOLESTEROL_HOMEOSTASIS
COAGULATION
WNT_BETA_CATENIN_SIGNALING
KRAS_SIGNALING_DN
GLYCOLYSIS
UV_RESPONSE_UP
HEDGEHOG_SIGNALING
NOTCH_SIGNALING
TGF_BETA_SIGNALING
UV_RESPONSE_DN
HYPOXIA
APICAL_JUNCTION
EPITHELIAL_MESENCHYMAL_TRANSITION
ANGIOGENESIS
P53_PATHWAY
TNFA_SIGNALING_VIA_NFKB
APOPTOSIS
KRAS_SIGNALING_UP
APICAL_SURFACE
MYOGENESIS
ESTROGEN_RESPONSE_EARLY
ESTROGEN_RESPONSE_LATE
REACTIVE_OXYGEN_SPECIES_PATHWAY
INTERFERON_ALPHA_RESPONSE
INTERFERON_GAMMA_RESPONSE
IL6_JAK_STAT3_SIGNALING
COMPLEMENT
ALLOGRAFT_REJECTION
INFLAMMATORY_RESPONSE
IL2_STAT5_SIGNALING
ANDROGEN_RESPONSE
PROTEIN_SECRETION
ADIPOGENESIS
HEME_METABOLISM
Expression
−2 −1 0 1 2
Cluster:
C1
C2
C3

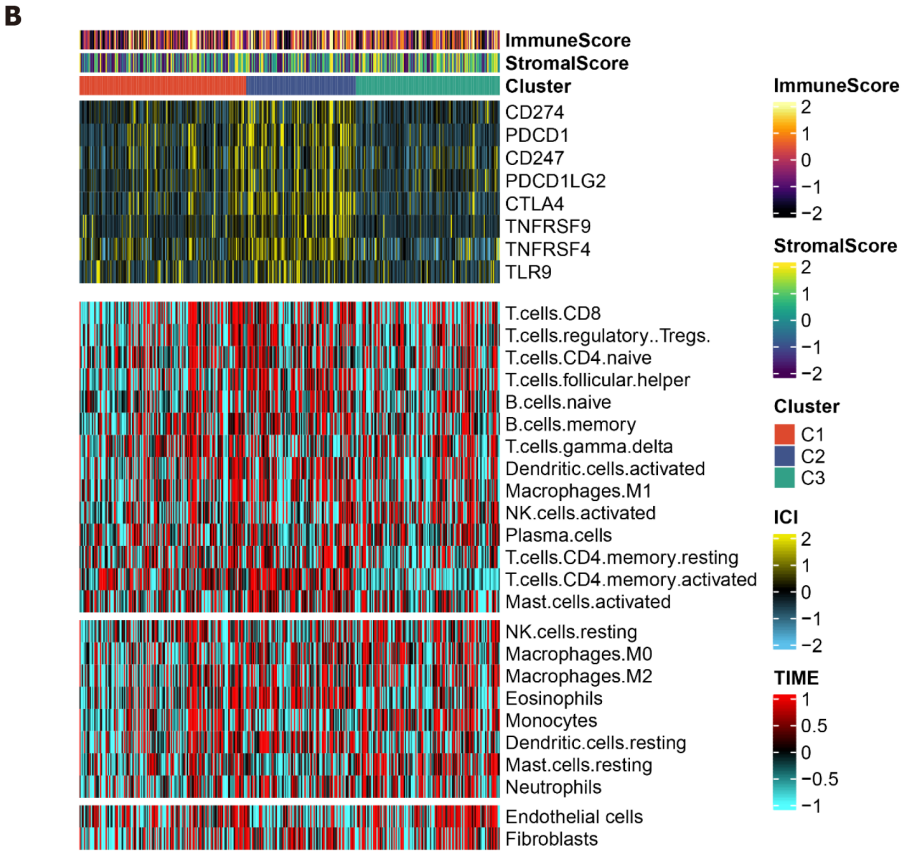
B
ImmuneScore
StromalScore
Cluster
CD274
PDCD1
CD247
PDCD1LG2
CTLA4
TNFRSF9
TNFRSF4
TLR9
T.cells.CD8
T.cells.regulatory..Tregs.
T.cells.CD4.naive
T.cells.follicular.helper
B.cells.naive
B.cells.memory
T.cells.gamma.delta
Dendritic.cells.activated
Macrophages.M1
NK.cells.activated
Plasma.cells
T.cells.CD4.memory.resting
T.cells.CD4.memory.activated
Mast.cells.activated
NK.cells.resting
Macrophages.M0
Macrophages.M2
Eosinophils
Monocytes
Dendritic.cells.resting
Mast.cells.resting
Neutrophils
Endothelial cells
Fibroblasts
ImmuneScore
2 1 0 −1 −2
StromalScore
2 1 0 −1 −2
Cluster
C1
C2
C3
ICI
2 1 0 −1 −2
TIME
1 0.5 0 −0.5 −1

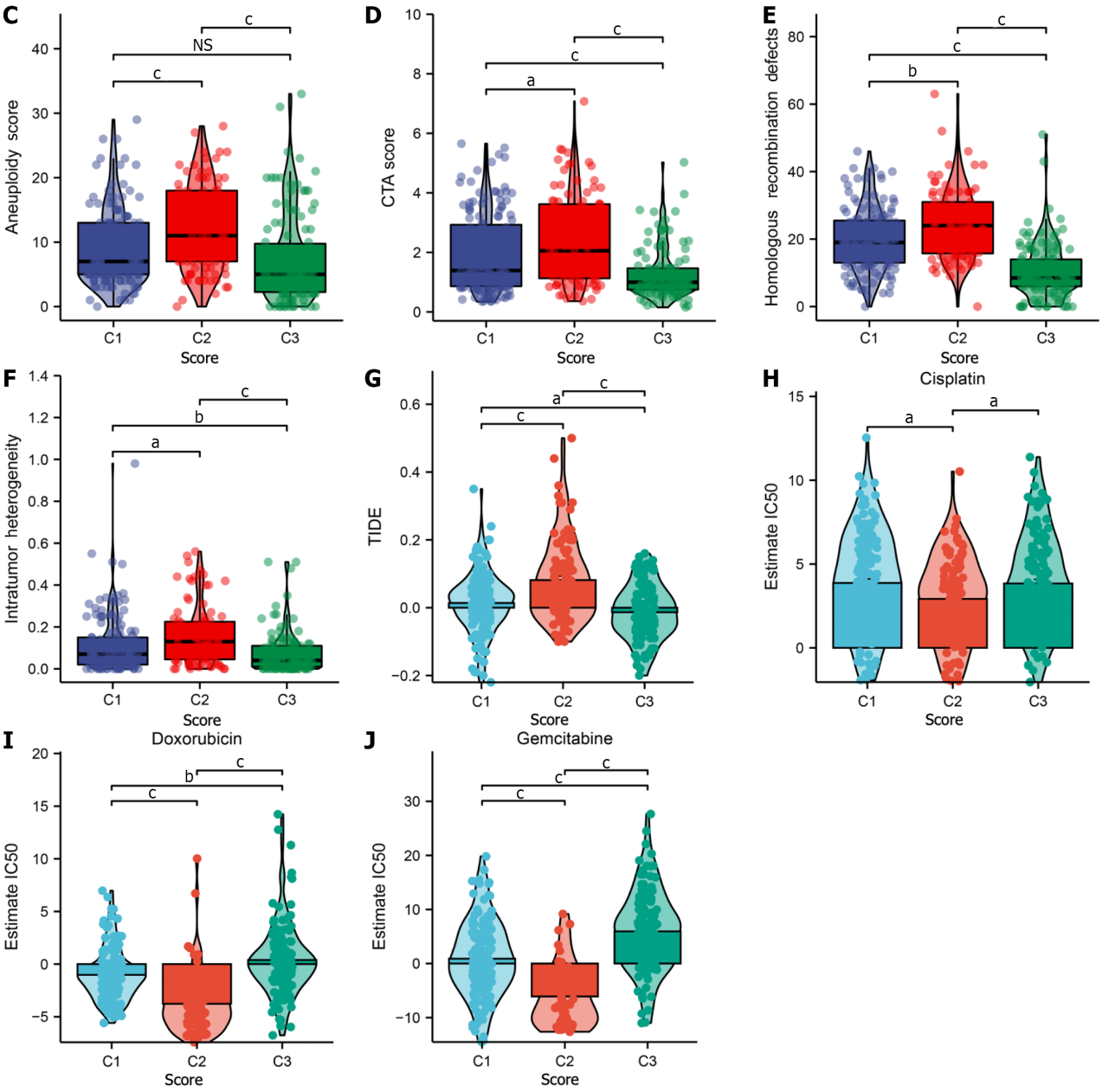

Figure 3 Immunogenomic landscape of three cellular senescence subtypes across TCGA-LIHC. A: The activity of 50 hallmark pathways in three subtypes; B: Abundance of the tumor microenvironment components, transcript levels of immune checkpoints, and stromal and immune scores across subtypes; C–F: Differences in aneuploidy score, cancer-testicular antigen score, homologous recombination defects, and intratumor heterogeneity between subtypes; G: Difference in TIDE score between subtypes; H–J: Differences in IC_{50} values of cisplatin, doxorubicin and gemcitabine between subtypes. [a]$P < 0.05$; [b]$P < 0.01$; [c]$P < 0.001$. NS: Not significant; TIDE: Tumor Immune Dysfunction and Exclusion.

progression[46]. G6PD weakens ferroptosis in HCC through targeting cytochrome P450 oxidoreductase[47]. PSRC1, a hypoxia- and immune-associated gene, associates with HCC survival[48]. The nonmetabolic role of UCK2 facilitates HCC metastasis *via* EGFR–AKT signaling activation[49]. TCOF1 coordinates oncogenic activation and rRNA generation as well as results in HCC initiation[50]. Clinical features of HCC patients are notably associated with survival outcomes. To better optimize the cellular-senescence-relevant gene signature and improve the prediction accuracy, we incorporated stage in combination with the cellular-senescence-relevant gene signature to build a nomogram that enabled us to generate the individual survival probability in HCC patients. High-RiskScore HCCs might respond to cisplatin, doxorubicin or gemcitabine, while low-RiskScore HCCs more possibly benefit from immunotherapy, proving the potential of the cellular-senescence-relevant gene signature in inferring therapeutic efficacy. Among the cellular-senescence-relevant genes, the expression and role of TRNP1 in HCC remain indistinct. Only bioinformatics evidence demonstrated the prognostic significance of TRNP1 in HCC[51]. Our study experimentally proved that TRNP1 was upregulated in HCC, and TRNP1 knockdown induced apoptosis and senescence of HCC cells and attenuated tumor growth. Thus, TRNP1 potentially participates in HCC senescence and progression, which might be a promising therapeutic target.

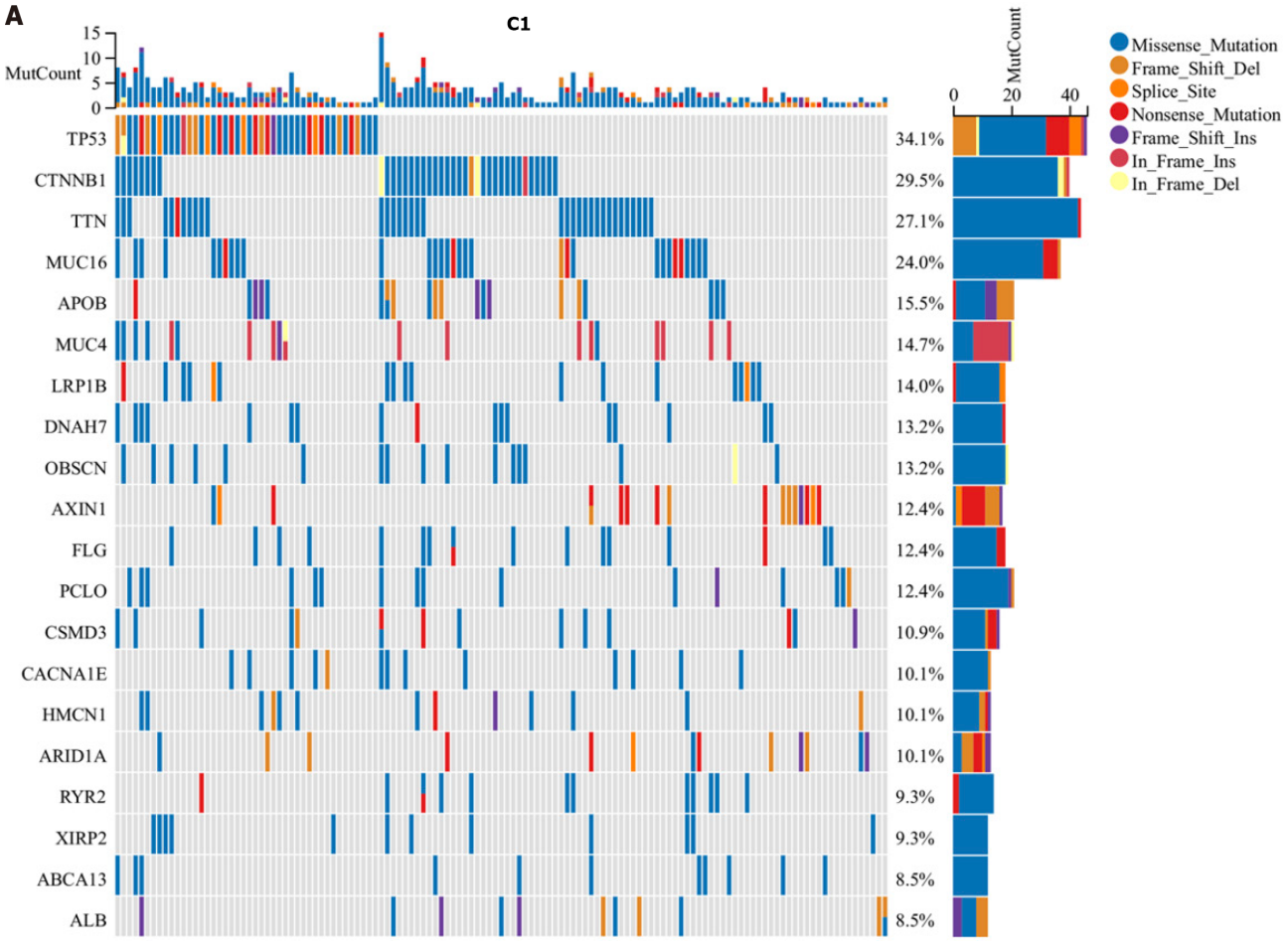
A
C1
MutCount
15
10
5
0
TP53 34.1%
CTNNB1 29.5%
TTN 27.1%
MUC16 24.0%
APOB 15.5%
MUC4 14.7%
LRP1B 14.0%
DNAH7 13.2%
OBSCN 13.2%
AXIN1 12.4%
FLG 12.4%
PCLO 12.4%
CSMD3 10.9%
CACNA1E 10.1%
HMCN1 10.1%
ARID1A 10.1%
RYR2 9.3%
XIRP2 9.3%
ABCA13 8.5%
ALB 8.5%
MutCount
0 20 40
Missense_Mutation
Frame_Shift_Del
Splice_Site
Nonsense_Mutation
Frame_Shift_Ins
In_Frame_Ins
In_Frame_Del

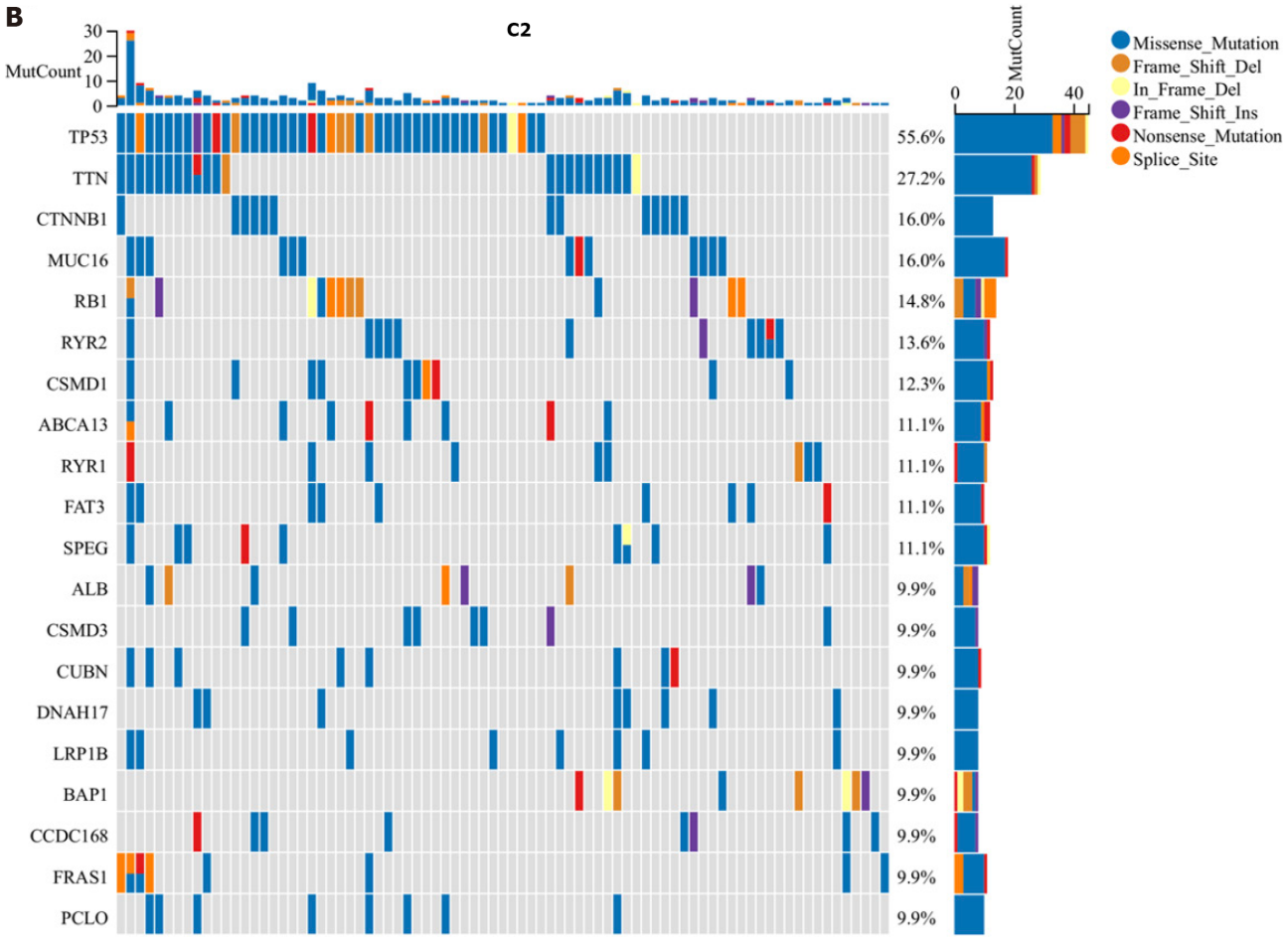
B
C2
MutCount
30
20
10
0
TP53 55.6%
TTN 27.2%
CTNNB1 16.0%
MUC16 16.0%
RB1 14.8%
RYR2 13.6%
CSMD1 12.3%
ABCA13 11.1%
RYR1 11.1%
FAT3 11.1%
SPEG 11.1%
ALB 9.9%
CSMD3 9.9%
CUBN 9.9%
DNAH17 9.9%
LRP1B 9.9%
BAP1 9.9%
CCDC168 9.9%
FRAS1 9.9%
PCLO 9.9%
MutCount
0 20 40
Missense_Mutation
Frame_Shift_Del
In_Frame_Del
Frame_Shift_Ins
Nonsense_Mutation
Splice_Site

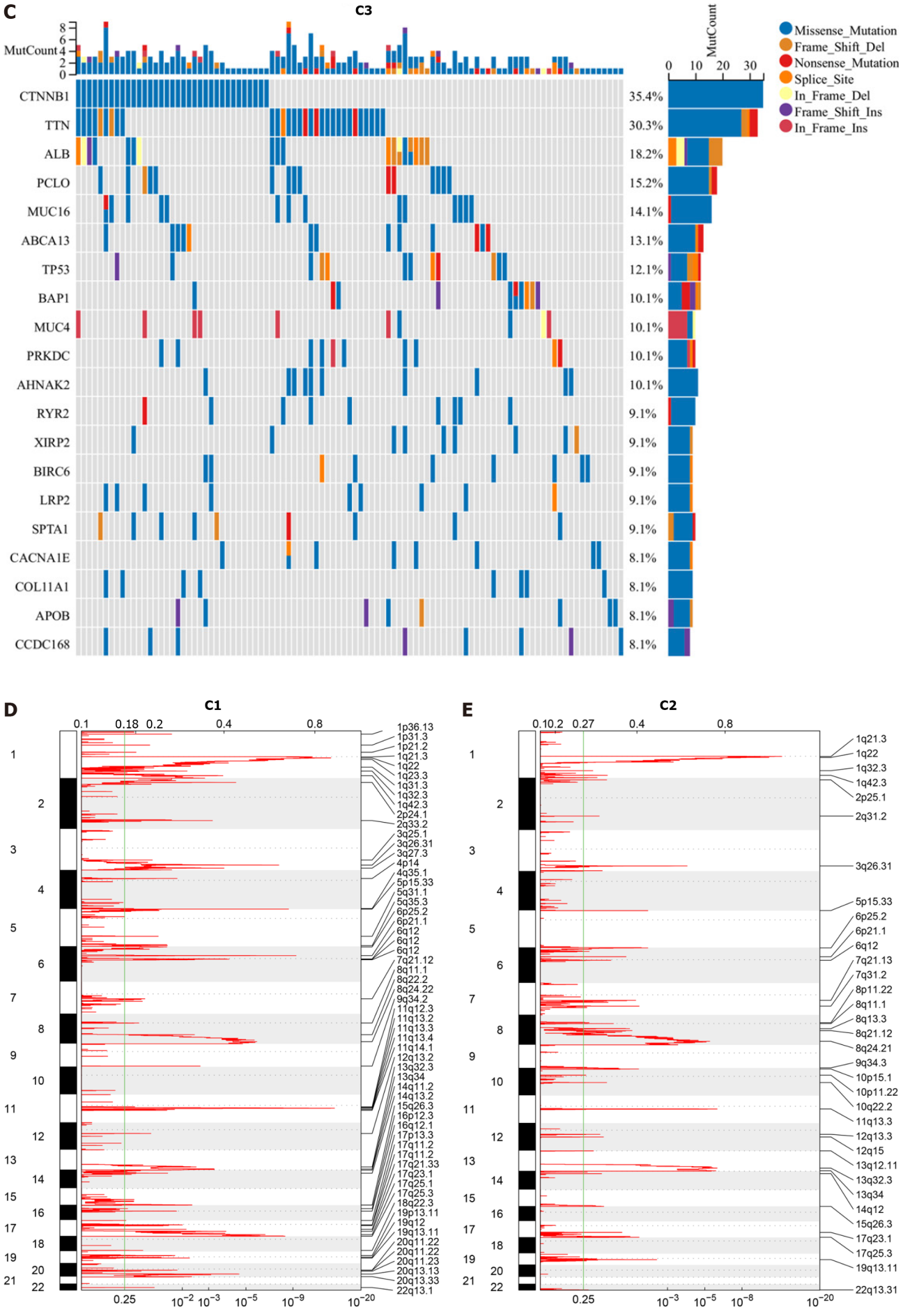
C
C3
MutCount
Missense_Mutation
Frame_Shift_Del
Nonsense_Mutation
Splice_Site
In_Frame_Del
Frame_Shift_Ins
In_Frame_Ins
CTNNB1 35.4%
TTN 30.3%
ALB 18.2%
PCLO 15.2%
MUC16 14.1%
ABCA13 13.1%
TP53 12.1%
BAP1 10.1%
MUC4 10.1%
PRKDC 10.1%
AHNAK2 10.1%
RYR2 9.1%
XIRP2 9.1%
BIRC6 9.1%
LRP2 9.1%
SPTA1 9.1%
CACNA1E 8.1%
COL11A1 8.1%
APOB 8.1%
CCDC168 8.1%
D
C1
E
C2

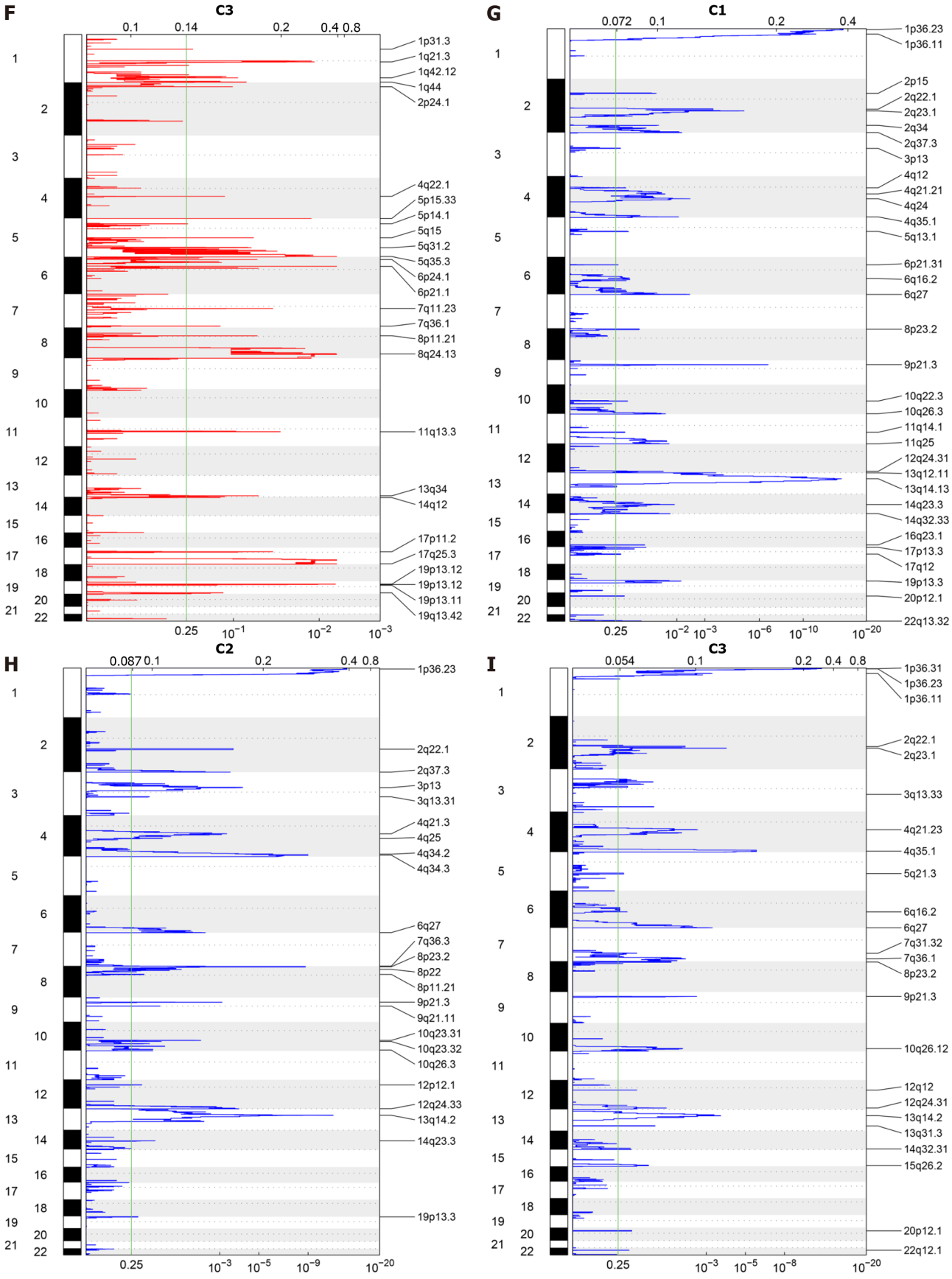

Figure 4 Genetic alterations of three cellular senescence subtypes. A–C: Significant mutated genes in The Cancer Genome Atlas hepatocellular carcinomas stratified by cellular senescence subtypes; D–F: Copy number amplification plots in three subtypes. The green line denotes the significance threshold (q = 0.25); G–I: Copy number deletion plots in three subtypes.

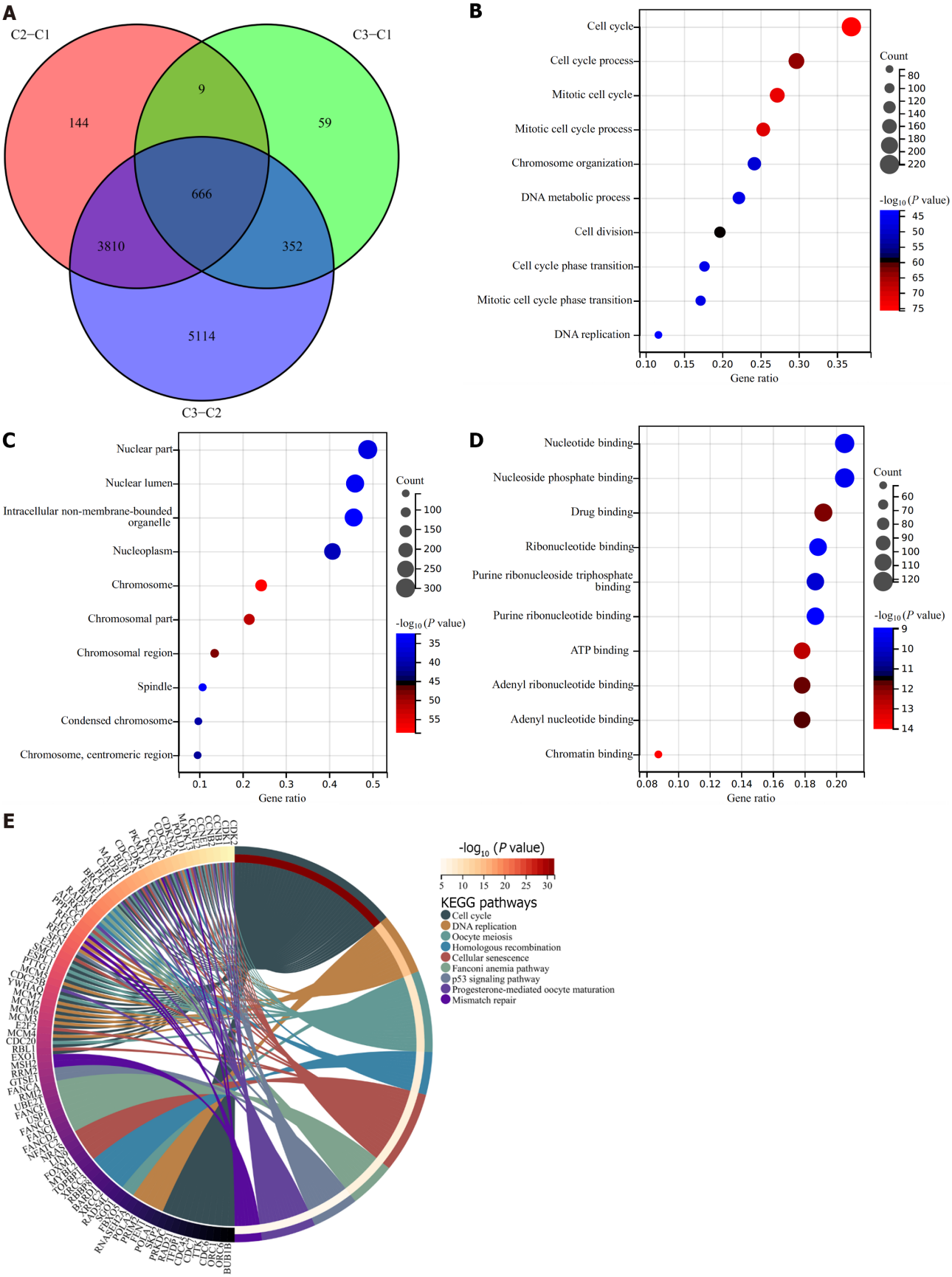

Figure 5 Identification of cellular senescence subtype-relevant genes and functional implications. A: Venn diagram of the intersected genes from differentially expressed genes between cellular senescence subtypes in TCGA-LIHC cohort; B–D: The top 10 biological processes, cellular components, together with molecular functions of cellular senescence subtype-relevant genes; E: Kyoto Encyclopedia of Genes and Genomes pathways significantly enriched by these genes.

Our study had some limitations. Due to the lack of HCC patients who received neoadjuvant immunotherapy, the relationship between cellular senescence subtypes and relevant gene signature with immunotherapeutic response requires further verification in the immunotherapy cohorts. Despite the external verification in the ICGC dataset, the predictive efficacy of cellular senescence-relevant gene signature needs to be proven in prospective cohorts.

CONCLUSION

Our findings showed the importance of cellular senescence in HCC classification and pharmacological interventions for clinical management. Additionally, we defined a cellular-senescence-relevant scoring system that can infer patient survival and therapeutic efficacy. Considering the clinically relevant parameters were closely linked with HCC survival, we incorporated stage in combination with the cellular-senescence-relevant gene signature to build a nomogram. Our integrated analysis provides a valuable framework for comprehending cellular senescence in HCC, which sheds light on the senescence-associated biomarker discovery as well as therapeutic targets.

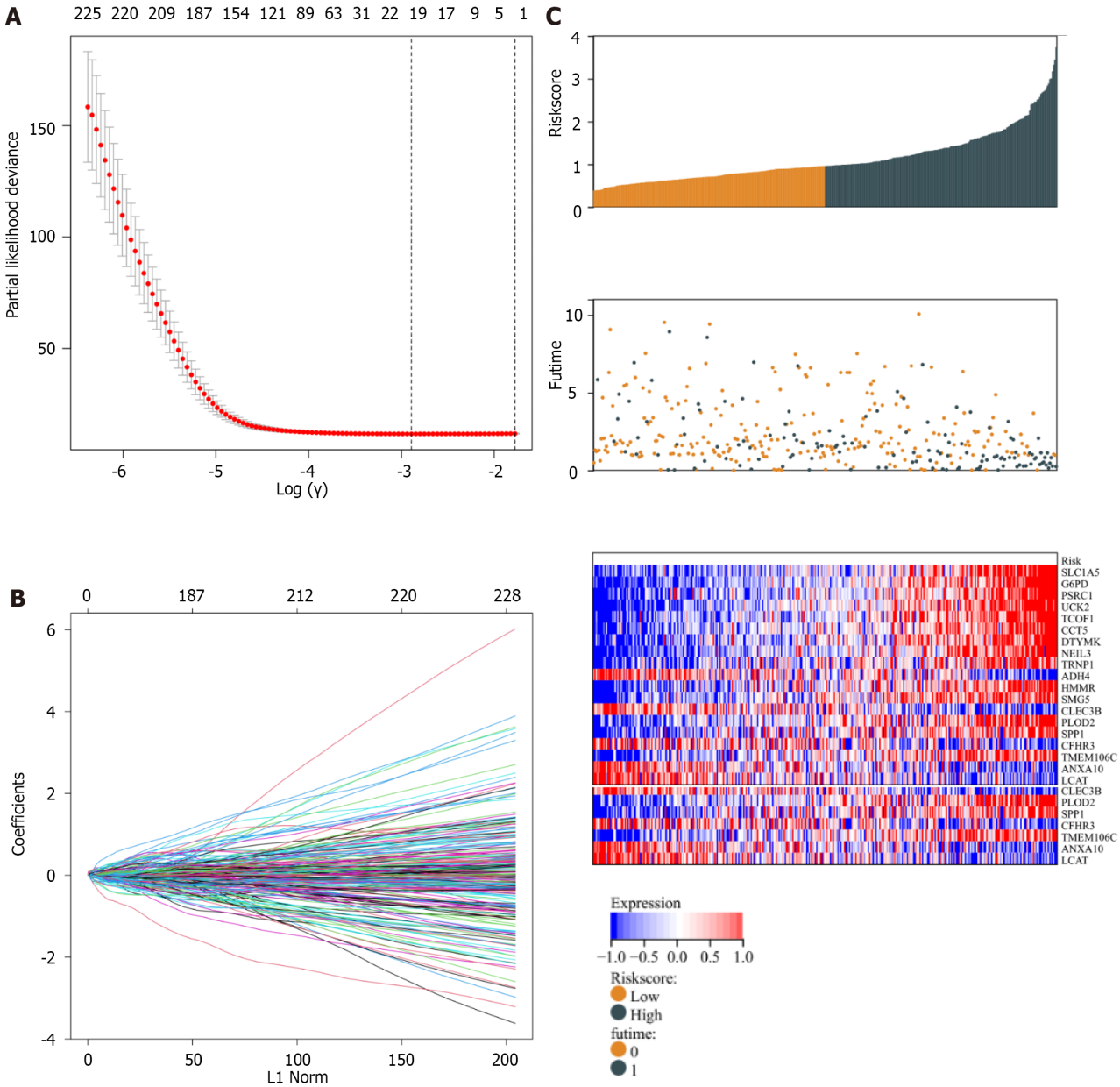

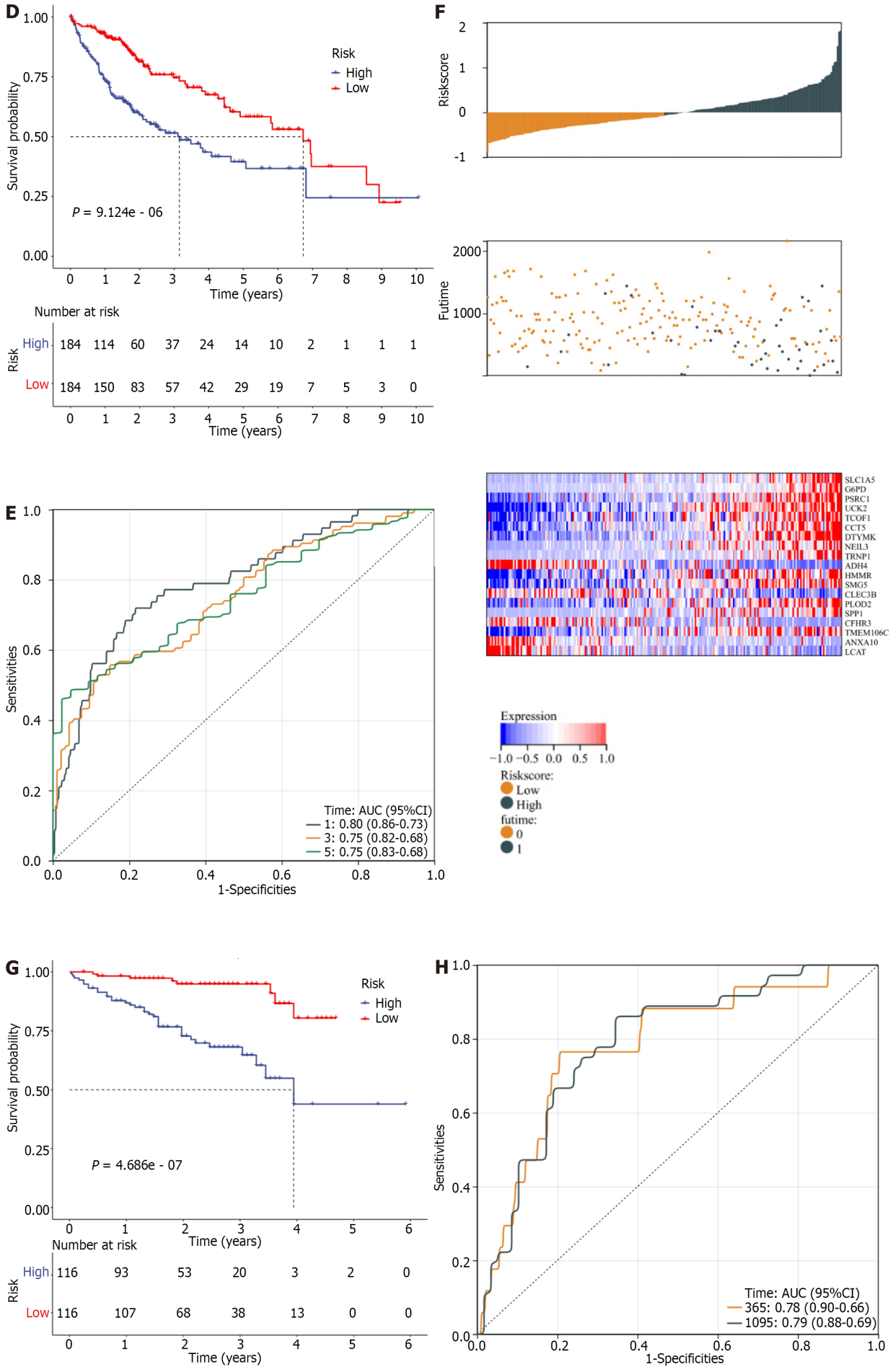
D
Survival probability
Risk
High
Low
P = 9.124e - 06
Time (years)
Number at risk
High 184 114 60 37 24 14 10 2 1 1 1
Low 184 150 83 57 42 29 19 7 5 3 0
F
Riskscore
Futime
E
Sensitivities
1-Specificities
Time: AUC (95%CI)
1: 0.80 (0.86-0.73)
3: 0.75 (0.82-0.68)
5: 0.75 (0.83-0.68)
SLC1A5
G6PD
PSRC1
UCK2
TCOF1
CCT5
DTYMK
NEIL3
TRNP1
ADH4
HMMR
SMG5
CLEC3B
PLOD2
SPP1
CFHR3
TMEM106C
ANXA10
LCAT
Expression
Riskscore:
Low
High
futime:
0
1
G
Survival probability
Risk
High
Low
P = 4.686e - 07
Number at risk
High 116 93 53 20 3 2 0
Low 116 107 68 38 13 0 0
Time (years)
H
Sensitivities
1-Specificities
Time: AUC (95%CI)
365: 0.78 (0.90-0.66)
1095: 0.79 (0.88-0.69)

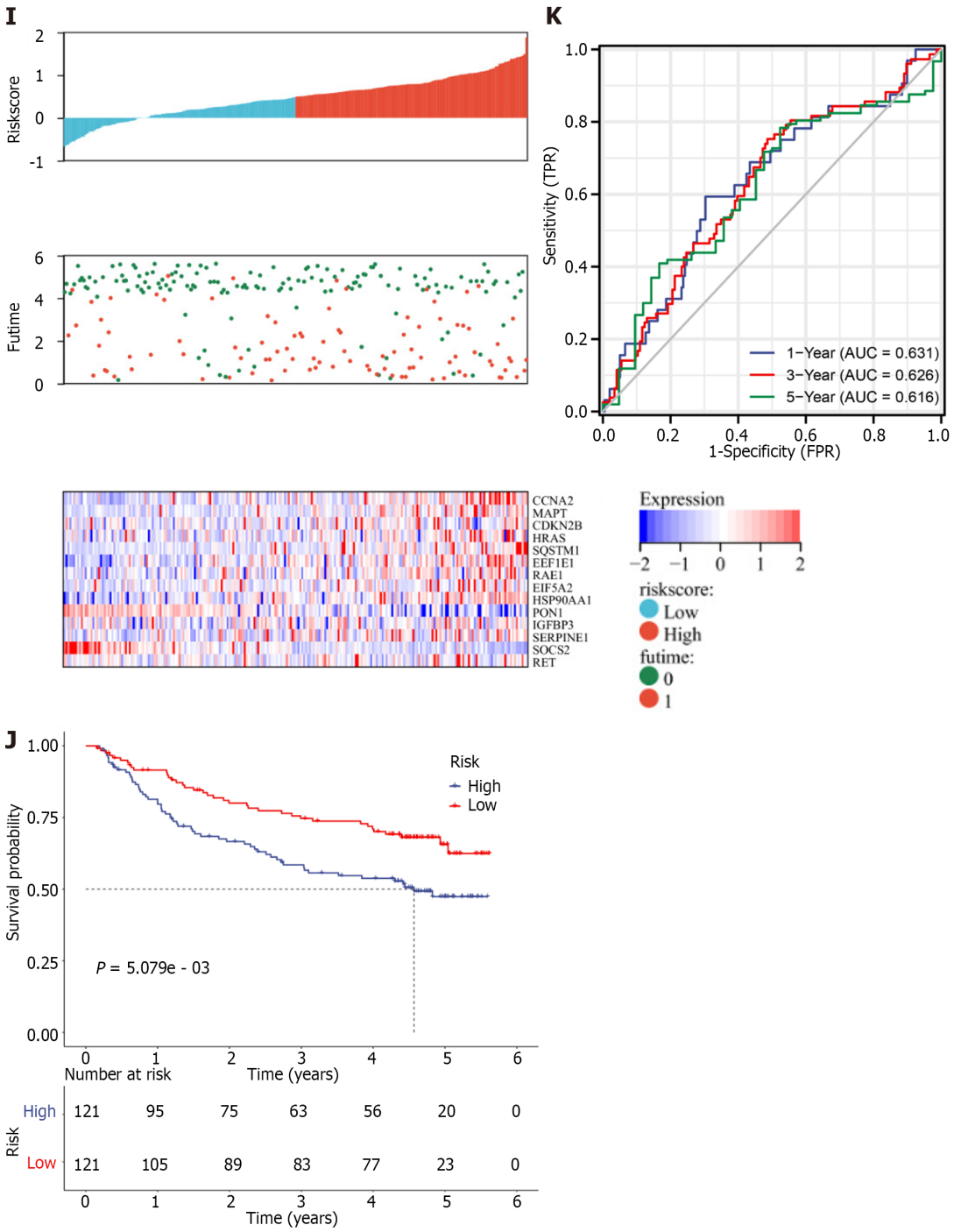

Figure 6 Definition and external verification of a cellular-senescence-relevant gene signature. A: Cross-validation for tuning the parameter selection in the least absolute shrinkage and selection operator (LASSO) analysis in TCGA-LIHC dataset; B: LASSO coefficient profiling; C: Distribution of RiskScore, survival status, and transcript levels of genes in the signature; D: Kaplan–Meier (curves of overall survival in low- and high-RiskScore hepatocellular carcinomas; E: Receiver operator characteristic curves (ROCs) at 1-, 3- and 5-year survival; F: External verification of distribution of RiskScore, survival status, and transcript levels of genes in the International Cancer Genome Consortium (ICGC) dataset; G: Kaplan–Meier curves of overall survival in two groups in the ICGC dataset; H: ROCs at 1- and 3-year survival based upon RiskScore in the ICGC dataset; I: External validation of distribution of RiskScore, survival status, and transcript levels of genes in the GSE14520 dataset; J: Kaplan–Meier curves of overall survival in two groups in the GSE14520 dataset; K: ROCs at 1- and 3-year survival in the GSE14520 dataset.

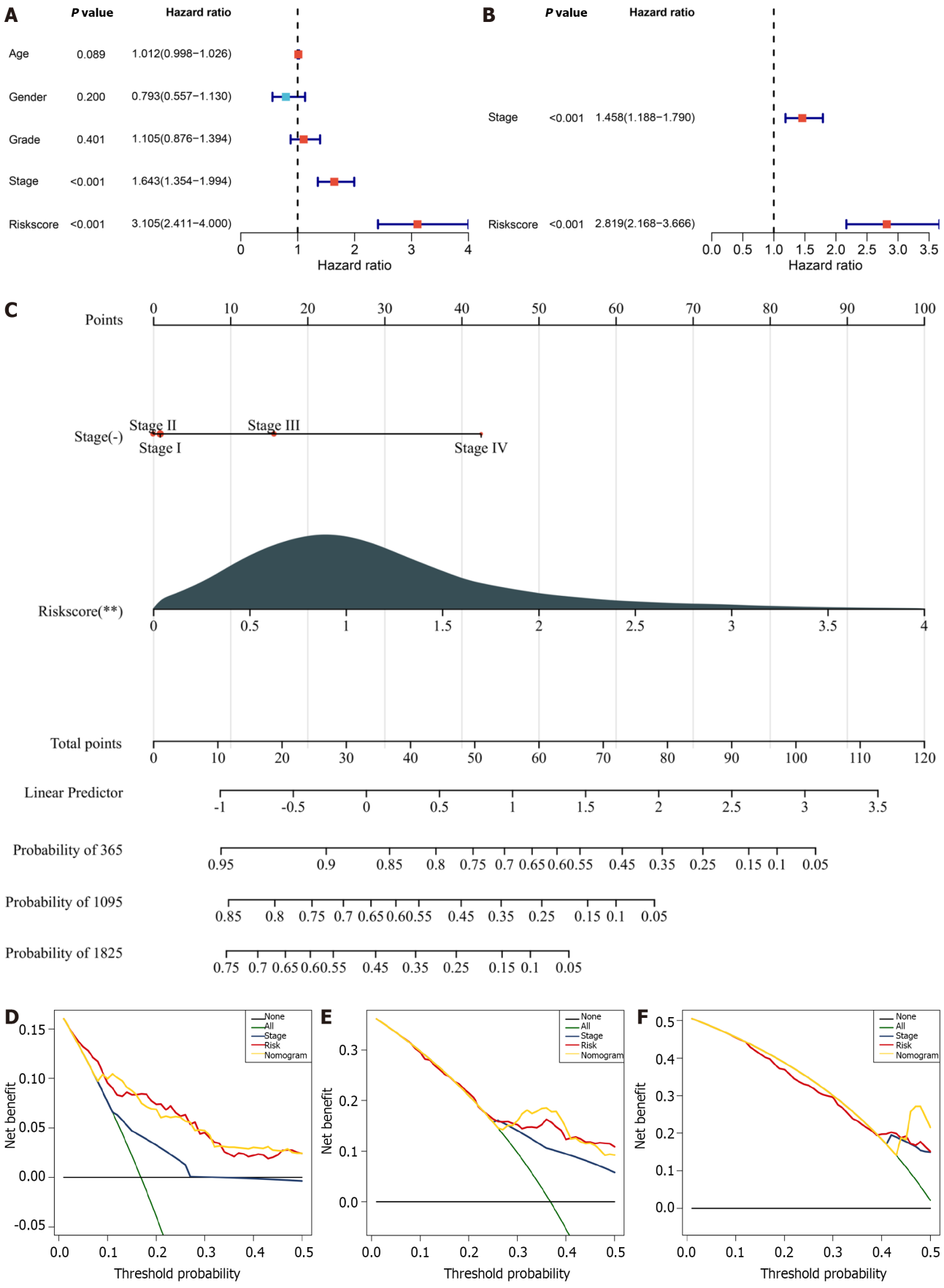

Figure 7 Establishment of a prognostic nomogram for clinical practice in the TCGA-LIHC dataset. A: Univariate-cox regression results of the cellular-senescence-relevant gene signature and conventional clinicopathological parameters with hepatocellular carcinoma prognosis; B: Multivariate Cox regression for selecting independent prognostic parameters; C: Generation of a nomogram based on stage and the cellular senescence-relevant RiskScore; D–F: Decision curve analysis at 1-, 1-, and 5-year survival.

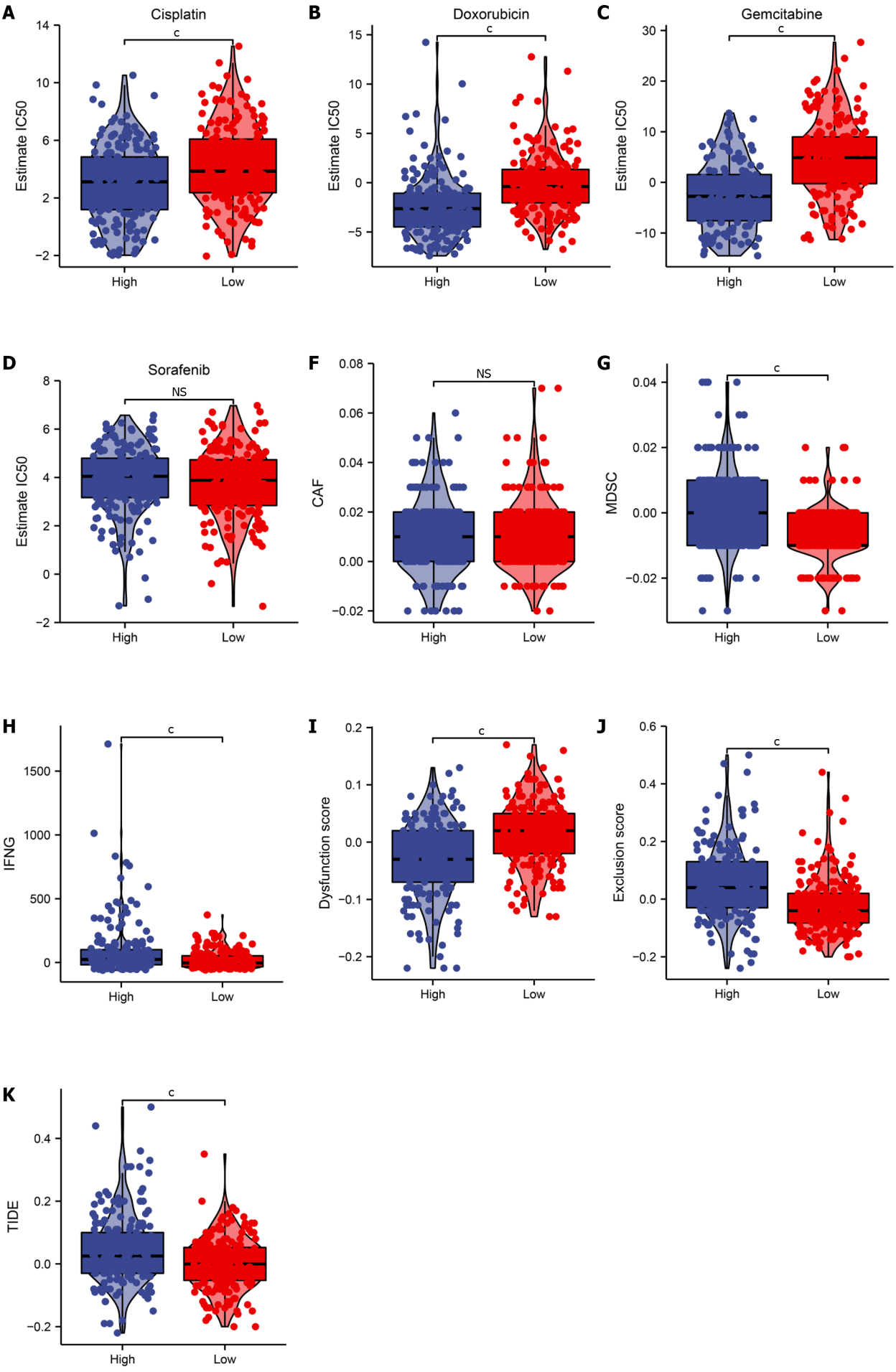
A
Cisplatin
Estimate IC50
c
High
Low
B
Doxorubicin
Estimate IC50
c
High
Low
C
Gemcitabine
Estimate IC50
c
High
Low
D
Sorafenib
Estimate IC50
NS
High
Low
F
CAF
NS
High
Low
G
MDSC
c
High
Low
H
IFNG
c
High
Low
I
Dysfunction score
c
High
Low
J
Exclusion score
c
High
Low
K
TIDE
c
High
Low

Figure 8 Assessment of the cellular senescence-relevant gene signature in predicting efficacy of pharmacological interventions in TCGA-LIHC dataset. A–D: IC_{50} value of cisplatin, doxorubicin, gemcitabine, and sorafenib in low- and high-RiskScore hepatocellular carcinomas (HCCs); E: Abundance of the tumor microenvironment components inferred by multiple algorithms; F–K: Comparison of carcinoma-associated fibroblast (CAF), myeloid-derived suppressor cell (MDSC), interferon gamma (IFNG), dysfunction score, exclusion score and Tumor Immune Dysfunction and Exclusion levels in low- and high-RiskScore HCCs. °P < 0.001. ns: No significant difference.

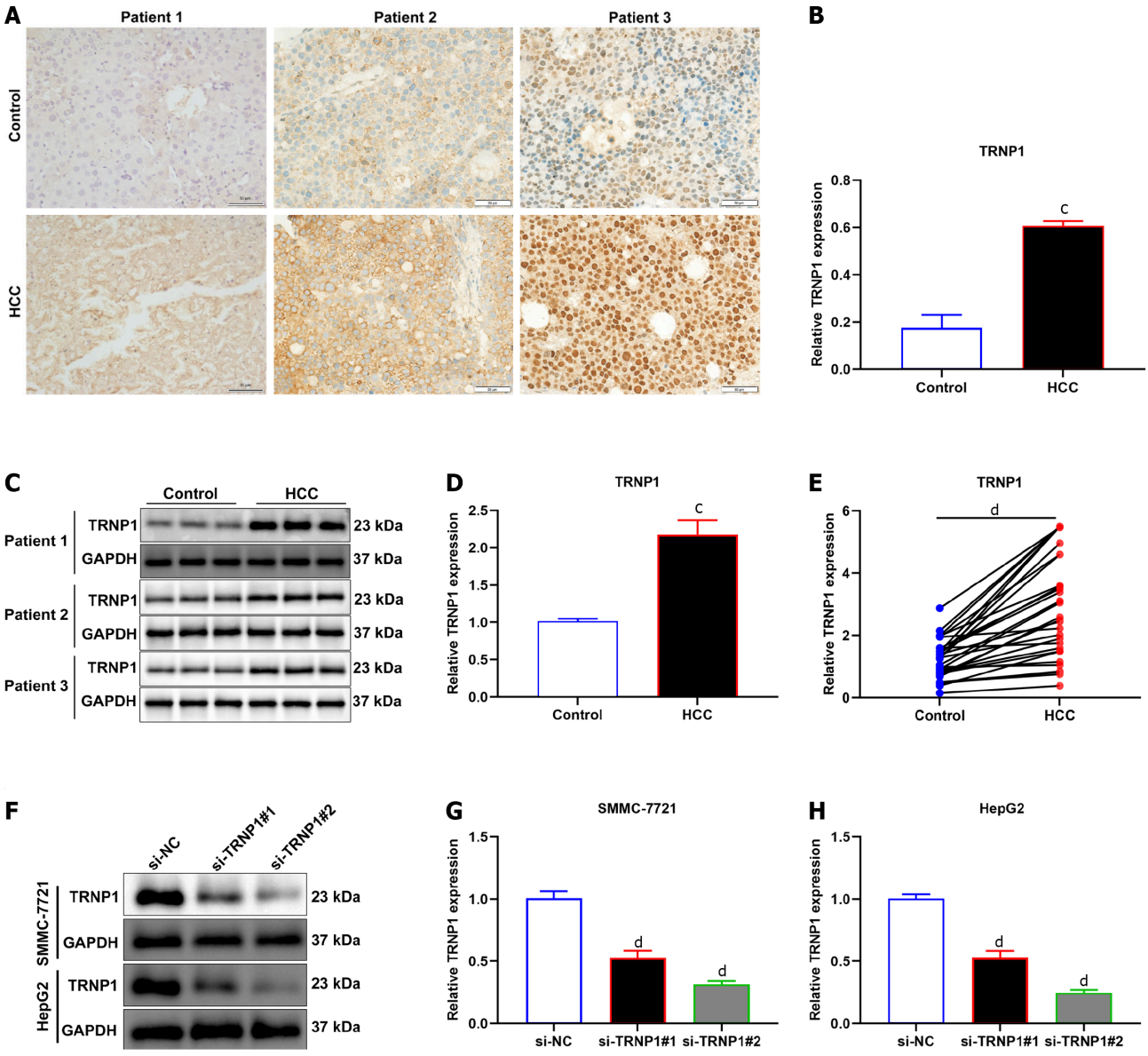

Figure 9 Experimental verification of expression of *TRNP1* in hepatocellular carcinomas. A and B: Representative immunohistochemistry of *TRNP1* expression in human hepatocellular carcinomas (HCCs) and normal tissues. Bar, 50 μm; C and D: Representative immunoblotting of *TRNP1* expression in human HCCs and normal tissues; E: Quantitative real-time polymerase chain reaction of *TRNP1* expression in 30 pairs of human HCCs and normal tissues; F–H: Immunoblotting of *TRNP1* expression in SMMC-7721 and HepG2 cells transfected with specific siRNAs of *TRNP1*. $^{c}P < 0.001$; $^{d}P < 0.0001$.

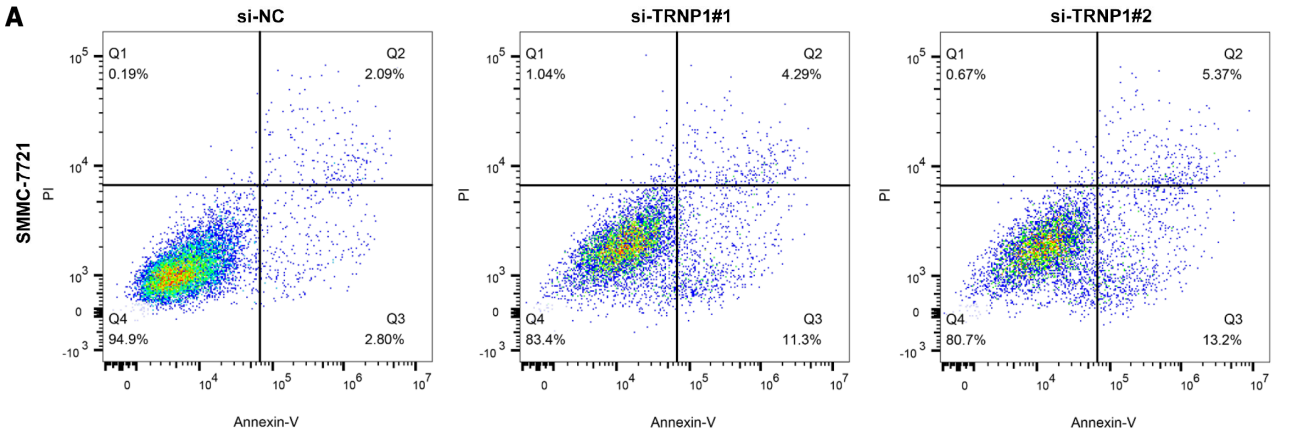

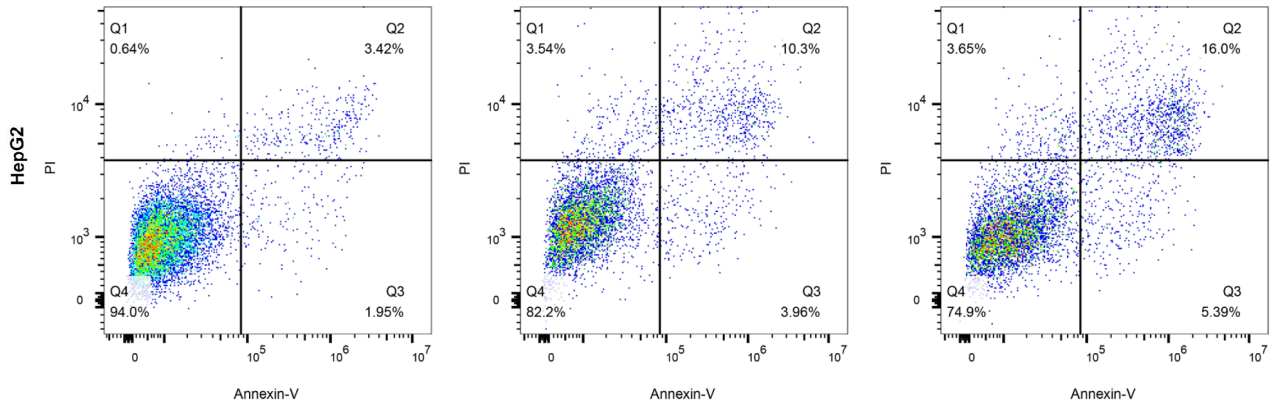
HepG2
Q1
0.64%
Q2
3.42%
Q4
94.0%
Q3
1.95%
Q1
3.54%
Q2
10.3%
Q4
82.2%
Q3
3.96%
Q1
3.65%
Q2
16.0%
Q4
74.9%
Q3
5.39%
PI
Annexin-V

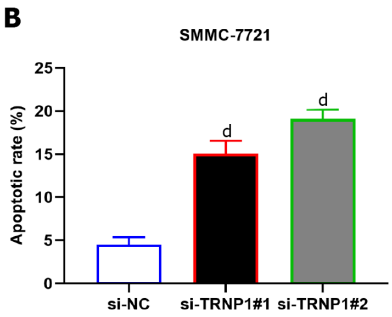
B
SMMC-7721
Apoptotic rate (%)
si-NC
si-TRNP1#1
si-TRNP1#2

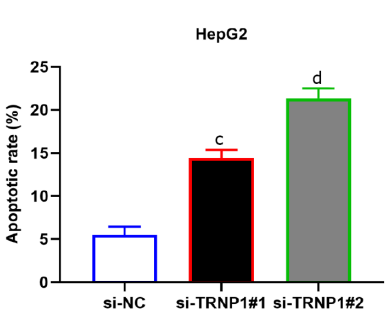
C
HepG2
Apoptotic rate (%)
si-NC
si-TRNP1#1
si-TRNP1#2

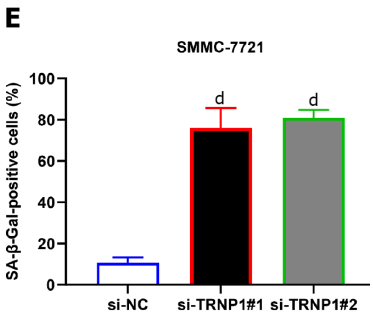
E
SMMC-7721
SA-β-Gal-positive cells (%)
si-NC
si-TRNP1#1
si-TRNP1#2

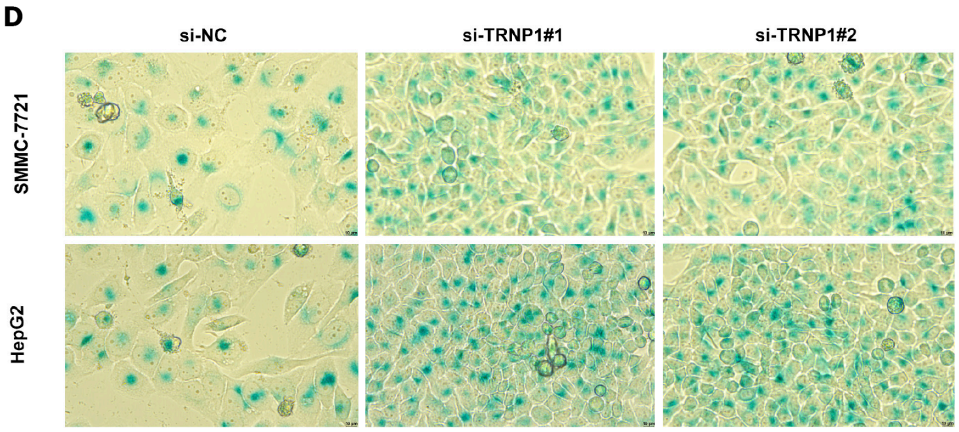
D
si-NC
si-TRNP1#1
si-TRNP1#2
SMMC-7721
HepG2

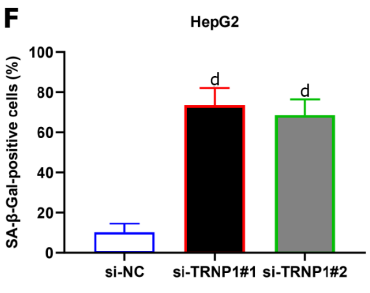
F
HepG2
SA-β-Gal-positive cells (%)
si-NC
si-TRNP1#1
si-TRNP1#2

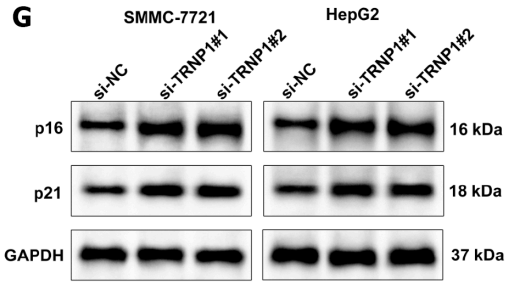
G
SMMC-7721
HepG2
si-NC
si-TRNP1#1
si-TRNP1#2
p16
16 kDa
p21
18 kDa
GAPDH
37 kDa

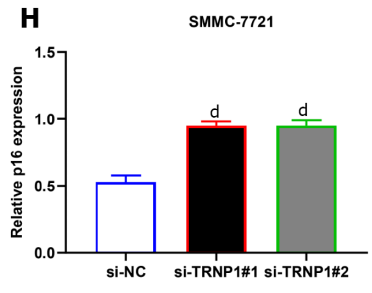
H
SMMC-7721
Relative p16 expression
si-NC
si-TRNP1#1
si-TRNP1#2

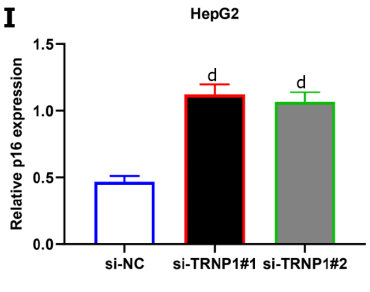
I
HepG2
Relative p16 expression
si-NC
si-TRNP1#1
si-TRNP1#2

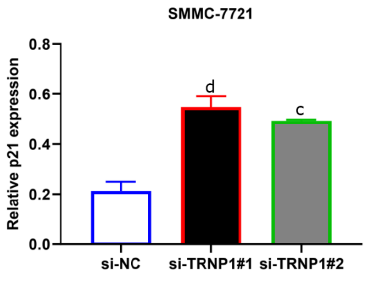
J
SMMC-7721
Relative p21 expression
si-NC
si-TRNP1#1
si-TRNP1#2

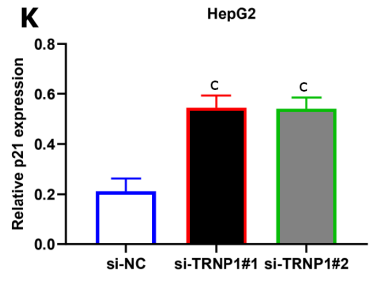
K
HepG2
Relative p21 expression
si-NC
si-TRNP1#1
si-TRNP1#2

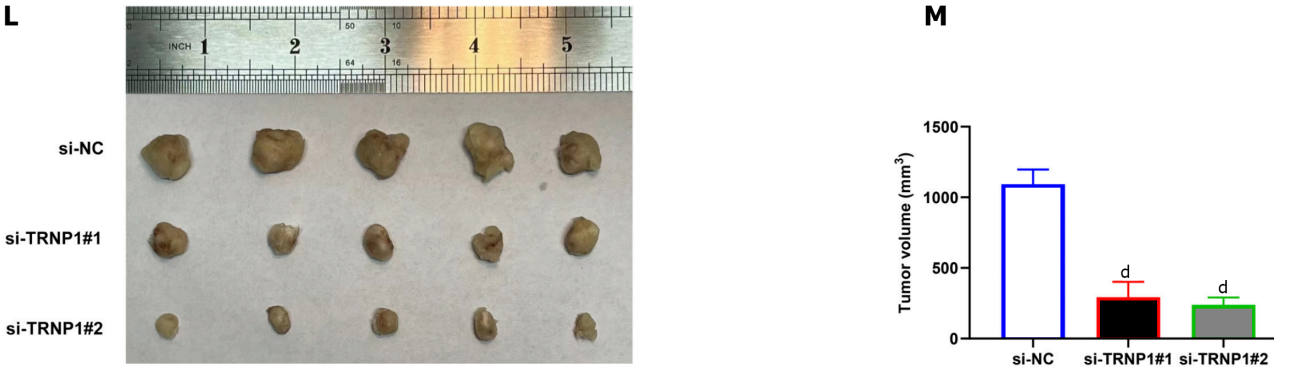

Figure 10 Suppression of TRNP1 induces apoptosis and senescence of hepatocellular carcinoma cells and attenuates tumor growth. A–C: Flow cytometry for measuring the apoptotic rate of in SMMC-7721 and HepG2 cells with transfection of specific siRNAs of TRNP1; D-F: SA-β-galactosidase (SA-β-Gal) staining for evaluating senescence of transfected hepatocellular carcinoma cells. Bar, 10 μm; G–K: Immunoblotting of p16 and p21 expression in transfected cells; L: Representative photographs of tumors from mice of si-NC, si-TRNP1#1 and si-TRNP1#2 groups; M: Calculation of tumor volume in above groups. $^{c}P < 0.001$; $^{d}P < 0.0001$.

ARTICLE HIGHLIGHTS

Research background

Cellular senescence, a state of stable growth arrest, is intertwined with human cancers. Due to the highly heterogeneous malignancy at the molecular and histological levels, characterization of cellular-senescence-based classification might facilitate the personalized treatment of hepatocellular carcinoma (HCC).

Research motivation

Nonetheless, the heterogeneity of cellular-senescence-related features makes the definition and targeting of treatment-induced senescent cells challenging.

Research objectives

This study aimed to characterize cellular-senescence-based phenotypes in HCC, and identify a novel cellular-senescence-related therapeutic target.

Research methods

We enrolled two HCC datasets, TCGA-LIHC and International Cancer Genome Consortium (ICGC). Unsupervised clustering was executed to probe tumor heterogeneity based upon cellular senescence genes. Least absolute shrinkage and selection operator algorithm was utilized to define a cellular-senescence-relevant scoring system. TRNP1 expression was measured in HCCs and normal tissues through immunohistochemistry, immunoblotting and quantitative real-time polymerase chain reaction. The influence of TRNP1 on HCC senescence and growth was proven *via* a series of experiments.

Research results

TCGA-LIHC patients were classified as three cellular senescence subtypes, named C1–3. The robustness and reproducibility of these subtypes were proven in the ICGC cohort. C2 had the worst overall survival, C1 the next, and C3 the best. C2 presented the highest levels of immune checkpoints, abundance of immune cells, and immunogenetic indicators. Thus, C2 might respond to immunotherapy. C2 had the lowest somatic mutation rate, while C1 presented the highest copy number variations. A cellular-senescence-relevant gene signature was generated, which can predict patient survival, and chemo- or immunotherapeutic response. Experimentally, it was proven that TRNP1 presented with remarkable upregulation in HCCs. TRNP1 knockdown induced apoptosis and senescence of HCC cells and attenuated tumor growth.

Research conclusions

These findings provide a systematic framework for assessing cellular senescence in HCC, which decode the tumor heterogeneity and tailor the pharmacological interventions to improve clinical management.

Research perspectives

Cellular senescence, a state of stable growth arrest, is implicated in human cancers. Nevertheless, characterization of cellular-senescence-associated phenotypes in HCC is still indistinct. Here, we proposed a novel cellular-senescence-based classification for HCC and identified TRNP1 as a novel therapeutic target.

FOOTNOTES

Author contributions: Wang HH and Chen WL contributed equally to this work; Li H conceived and designed the study; Wang HH and Chen WL conducted most of the experiments and data analysis, and wrote the manuscript; Cui YY and Gong HH participated in collecting data and helped to draft the manuscript; All authors reviewed and approved the manuscript.

Supported by Project of Bozhou Municipal Health Commission, No. bzwj2022A001; Project of Bozhou Science and Technology Bureau, No. bzzc2022008; and Scientific Research Fund of Bozhou Hospital, Anhui Medical University, No. by2022001.

Institutional review board statement: The study was approved by the Ethics Committee of The Affiliated Bozhou Hospital of Anhui Medical University, No. 2022-17.

Informed consent statement: All study participants or their legal guardian provided informed written consent about personal and medical data collection prior to study enrolment.

Conflict-of-interest statement: The authors declare no conflicts of interest.

Data sharing statement: The data used to support the findings of this study are included within the supplementary information files.

Country/Territory of origin: China

ORCID number: Heng Li 0000-0002-6663-1046.

S-Editor: Fan JR
L-Editor: Kerr C
P-Editor: Zhang XD

REFERENCES

1 **Yamamoto-Imoto H**, Minami S, Shioda T, Yamashita Y, Sakai S, Maeda S, Yamamoto T, Oki S, Takashima M, Yamamuro T, Yanagawa K, Edahiro R, Iwatani M, So M, Tokumura A, Abe T, Imamura R, Nonomura N, Okada Y, Ayer DE, Ogawa H, Hara E, Takabatake Y, Isaka Y, Nakamura S, Yoshimori T. Age-associated decline of MondoA drives cellular senescence through impaired autophagy and mitochondrial homeostasis. *Cell Rep* 2022; **38**: 110444 [PMID: 35235784 DOI: 10.1016/j.celrep.2022.110444]

2 **Zhang D**, Liu Y, Zhu Y, Zhang Q, Guan H, Liu S, Chen S, Mei C, Chen C, Liao Z, Xi Y, Ouyang S, Feng XH, Liang T, Shen L, Xu P. A non-canonical cGAS-STING-PERK pathway facilitates the translational program critical for senescence and organ fibrosis. *Nat Cell Biol* 2022; **24**: 766-782 [PMID: 35501370 DOI: 10.1038/s41556-022-00894-z]

3 **Avelar RA**, Ortega JG, Tacutu R, Tyler EJ, Bennett D, Binetti P, Budovsky A, Chatsirisupachai K, Johnson E, Murray A, Shields S, Tejada-Martinez D, Thornton D, Fraifeld VE, Bishop CL, de Magalhães JP. A multidimensional systems biology analysis of cellular senescence in aging and disease. *Genome Biol* 2020; **21**: 91 [PMID: 32264951 DOI: 10.1186/s13059-020-01990-9]

4 **Chatsirisupachai K**, Palmer D, Ferreira S, de Magalhães JP. A human tissue-specific transcriptomic analysis reveals a complex relationship between aging, cancer, and cellular senescence. *Aging Cell* 2019; **18**: e13041 [PMID: 31560156 DOI: 10.1111/acel.13041]

5 **Laphanuwat P**, Gomes DCO, Akbar AN. Senescent T cells: Beneficial and detrimental roles. *Immunol Rev* 2023; **316**: 160-175 [PMID: 37098109 DOI: 10.1111/imr.13206]

6 **Lee DA**. Cellular therapy: Adoptive immunotherapy with expanded natural killer cells. *Immunol Rev* 2019; **290**: 85-99 [PMID: 31355489 DOI: 10.1111/imr.12793]

7 **Wang X**, Ma L, Pei X, Wang H, Tang X, Pei JF, Ding YN, Qu S, Wei ZY, Wang HY, Wang X, Wei GH, Liu DP, Chen HZ. Comprehensive assessment of cellular senescence in the tumor microenvironment. *Brief Bioinform* 2022; **23** [PMID: 35419596 DOI: 10.1093/bib/bbac118]

8 **Wang B**, Demaria M. The Quest to Define and Target Cellular Senescence in Cancer. *Cancer Res* 2021; **81**: 6087-6089 [PMID: 34911777 DOI: 10.1158/0008-5472.CAN-21-2032]

9 **Basu A**. The interplay between apoptosis and cellular senescence: Bcl-2 family proteins as targets for cancer therapy. *Pharmacol Ther* 2022; **230**: 107943 [PMID: 34182005 DOI: 10.1016/j.pharmthera.2021.107943]

10 **Wang L**, Lankhorst L, Bernards R. Exploiting senescence for the treatment of cancer. *Nat Rev Cancer* 2022; **22**: 340-355 [PMID: 35241831 DOI: 10.1038/s41568-022-00450-9]

11 **Sung H**, Ferlay J, Siegel RL, Laversanne M, Soerjomataram I, Jemal A, Bray F. Global Cancer Statistics 2020: GLOBOCAN Estimates of Incidence and Mortality Worldwide for 36 Cancers in 185 Countries. *CA Cancer J Clin* 2021; **71**: 209-249 [PMID: 33538338 DOI: 10.3322/caac.21660]

12 **Yau T**, Kang YK, Kim TY, El-Khoueiry AB, Santoro A, Sangro B, Melero I, Kudo M, Hou MM, Matilla A, Tovoli F, Knox JJ, Ruth He A, El-Rayes BF, Acosta-Rivera M, Lim HY, Neely J, Shen Y, Wisniewski T, Anderson J, Hsu C. Efficacy and Safety of Nivolumab Plus Ipilimumab in Patients With Advanced Hepatocellular Carcinoma Previously Treated With Sorafenib: The CheckMate 040 Randomized Clinical Trial. *JAMA Oncol* 2020; **6**: e204564 [PMID: 33001135 DOI: 10.1001/jamaoncol.2020.4564]

13 **Krstic J**, Reinisch I, Schindlmaier K, Galhuber M, Riahi Z, Berger N, Kupper N, Moyschewitz E, Auer M, Michenthaler H, Nössing C,

Depaoli MR, Ramadani-Muja J, Usluer S, Stryeck S, Pichler M, Rinner B, Deutsch AJA, Reinisch A, Madl T, Chiozzi RZ, Heck AJR, Huch M, Malli R, Prokesch A. Fasting improves therapeutic response in hepatocellular carcinoma through p53-dependent metabolic synergism. *Sci Adv* 2022; **8**: eabh2635 [PMID: 35061544 DOI: 10.1126/sciadv.abh2635]

14 **Kang YK**, Chen LT, Ryu MH, Oh DY, Oh SC, Chung HC, Lee KW, Omori T, Shitara K, Sakuramoto S, Chung IJ, Yamaguchi K, Kato K, Sym SJ, Kadowaki S, Tsuji K, Chen JS, Bai LY, Oh SY, Choda Y, Yasui H, Takeuchi K, Hirashima Y, Hagihara S, Boku N. Nivolumab plus chemotherapy versus placebo plus chemotherapy in patients with HER2-negative, untreated, unresectable advanced or recurrent gastric or gastro-oesophageal junction cancer (ATTRACTION-4): a randomised, multicentre, double-blind, placebo-controlled, phase 3 trial. *Lancet Oncol* 2022; **23**: 234-247 [PMID: 35030335 DOI: 10.1016/S1470-2045(21)00692-6]

15 **Liu X**, Niu X, Qiu Z. A Five-Gene Signature Based on Stromal/Immune Scores in the Tumor Microenvironment and Its Clinical Implications for Liver Cancer. *DNA Cell Biol* 2020; **39**: 1621-1638 [PMID: 32758021 DOI: 10.1089/dna.2020.5512]

16 **Xiang X**, Fu Y, Zhao K, Miao R, Zhang X, Ma X, Liu C, Zhang N, Qu K. Cellular senescence in hepatocellular carcinoma induced by a long non-coding RNA-encoded peptide PINT87aa by blocking FOXM1-mediated PHB2. *Theranostics* 2021; **11**: 4929-4944 [PMID: 33754036 DOI: 10.7150/thno.55672]

17 **Liu B**, Yi J, Yang X, Liu L, Lou X, Zhang Z, Qi H, Wang Z, Zou J, Zhu WG, Gu W, Luo J. MDM2-mediated degradation of WRN promotes cellular senescence in a p53-independent manner. *Oncogene* 2019; **38**: 2501-2515 [PMID: 30532073 DOI: 10.1038/s41388-018-0605-5]

18 **Paradis V**, Youssef N, Dargère D, Bâ N, Bonvoust F, Deschatrette J, Bedossa P. Replicative senescence in normal liver, chronic hepatitis C, and hepatocellular carcinomas. *Hum Pathol* 2001; **32**: 327-332 [PMID: 11274643 DOI: 10.1053/hupa.2001.22747]

19 **Liu B**, Zhou Z, Jin Y, Lu J, Feng D, Peng R, Sun H, Mu X, Li C, Chen Y. Hepatic stellate cell activation and senescence induced by intrahepatic microbiota disturbances drive progression of liver cirrhosis toward hepatocellular carcinoma. *J Immunother Cancer* 2022; **10** [PMID: 34996812 DOI: 10.1136/jitc-2021-003069]

20 **Yildiz G**, Arslan-Ergul A, Bagislar S, Konu O, Yuzugullu H, Gursoy-Yuzugullu O, Ozturk N, Ozen C, Ozdag H, Erdal E, Karademir S, Sagol O, Mizrak D, Bozkaya H, Ilk HG, Ilk O, Bilen B, Cetin-Atalay R, Akar N, Ozturk M. Genome-wide transcriptional reorganization associated with senescence-to-immortality switch during human hepatocellular carcinogenesis. *PLoS One* 2013; **8**: e64016 [PMID: 23691139 DOI: 10.1371/journal.pone.0064016]

21 **Eggert T**, Wolter K, Ji J, Ma C, Yevsa T, Klotz S, Medina-Echeverz J, Longerich T, Forgues M, Reisinger F, Heikenwalder M, Wang XW, Zender L, Greten TF. Distinct Functions of Senescence-Associated Immune Responses in Liver Tumor Surveillance and Tumor Progression. *Cancer Cell* 2016; **30**: 533-547 [PMID: 27728804 DOI: 10.1016/j.ccell.2016.09.003]

22 **Yu X**, Chen P, Yi W, Ruan W, Xiong X. Identification of cell senescence molecular subtypes in prediction of the prognosis and immunotherapy of hepatitis B virus-related hepatocellular carcinoma. *Front Immunol* 2022; **13**: 1029872 [PMID: 36275676 DOI: 10.3389/fimmu.2022.1029872]

23 **Luo Y**, Liu H, Fu H, Ding GS, Teng F. A cellular senescence-related classifier based on a tumorigenesis- and immune infiltration-guided strategy can predict prognosis, immunotherapy response, and candidate drugs in hepatocellular carcinoma. *Front Immunol* 2022; **13**: 974377 [PMID: 36458010 DOI: 10.3389/fimmu.2022.974377]

24 **Wang Z**, Yao J, Dong T, Niu X. Definition of a Novel Cuproptosis-Relevant lncRNA Signature for Uncovering Distinct Survival, Genomic Alterations, and Treatment Implications in Lung Adenocarcinoma. *J Immunol Res* 2022; **2022**: 2756611 [PMID: 36281357 DOI: 10.1155/2022/2756611]

25 **Yu G**, Wang LG, Han Y, He QY. clusterProfiler: an R package for comparing biological themes among gene clusters. *OMICS* 2012; **16**: 284-287 [PMID: 22455463 DOI: 10.1089/omi.2011.0118]

26 **Hänzelmann S**, Castelo R, Guinney J. GSVA: gene set variation analysis for microarray and RNA-seq data. *BMC Bioinformatics* 2013; **14**: 7 [PMID: 23323831 DOI: 10.1186/1471-2105-14-7]

27 **Liberzon A**, Birger C, Thorvaldsdóttir H, Ghandi M, Mesirov JP, Tamayo P. The Molecular Signatures Database (MSigDB) hallmark gene set collection. *Cell Syst* 2015; **1**: 417-425 [PMID: 26771021 DOI: 10.1016/j.cels.2015.12.004]

28 **Wilkerson MD**, Hayes DN. ConsensusClusterPlus: a class discovery tool with confidence assessments and item tracking. *Bioinformatics* 2010; **26**: 1572-1573 [PMID: 20427518 DOI: 10.1093/bioinformatics/btq170]

29 **Eide PW**, Bruun J, Lothe RA, Sveen A. CMScaller: an R package for consensus molecular subtyping of colorectal cancer pre-clinical models. *Sci Rep* 2017; **7**: 16618 [PMID: 29192179 DOI: 10.1038/s41598-017-16747-x]

30 **Mayakonda A**, Lin DC, Assenov Y, Plass C, Koeffler HP. Maftools: efficient and comprehensive analysis of somatic variants in cancer. *Genome Res* 2018; **28**: 1747-1756 [PMID: 30341162 DOI: 10.1101/gr.239244.118]

31 **Mermel CH**, Schumacher SE, Hill B, Meyerson ML, Beroukhim R, Getz G. GISTIC2.0 facilitates sensitive and confident localization of the targets of focal somatic copy-number alteration in human cancers. *Genome Biol* 2011; **12**: R41 [PMID: 21527027 DOI: 10.1186/gb-2011-12-4-r41]

32 **Engebretsen S**, Bohlin J. Statistical predictions with glmnet. *Clin Epigenetics* 2019; **11**: 123 [PMID: 31443682 DOI: 10.1186/s13148-019-0730-1]

33 **Chen L**, Niu X, Qiao X, Liu S, Ma H, Shi X, He X, Zhong M. Characterization of Interplay Between Autophagy and Ferroptosis and Their Synergistical Roles on Manipulating Immunological Tumor Microenvironment in Squamous Cell Carcinomas. *Front Immunol* 2021; **12**: 739039 [PMID: 35185859 DOI: 10.3389/fimmu.2021.739039]

34 **Geeleher P**, Cox N, Huang RS. pRRophetic: an R package for prediction of clinical chemotherapeutic response from tumor gene expression levels. *PLoS One* 2014; **9**: e107468 [PMID: 25229481 DOI: 10.1371/journal.pone.0107468]

35 **Jiang P**, Gu S, Pan D, Fu J, Sahu A, Hu X, Li Z, Traugh N, Bu X, Li B, Liu J, Freeman GJ, Brown MA, Wucherpfennig KW, Liu XS. Signatures of T cell dysfunction and exclusion predict cancer immunotherapy response. *Nat Med* 2018; **24**: 1550-1558 [PMID: 30127393 DOI: 10.1038/s41591-018-0136-1]

36 **Tao L**, Zhang W, Zhang Y, Zhang M, Niu X, Zhao Q, Liu Z, Li Y, Diao A. Caffeine promotes the expression of telomerase reverse transcriptase to regulate cellular senescence and aging. *Food Funct* 2021; **12**: 2914-2924 [PMID: 33720241 DOI: 10.1039/d0fo03246h]

37 **Chand V**, Liao X, Guzman G, Benevolenskaya E, Raychaudhuri P. Hepatocellular carcinoma evades RB1-induced senescence by activating the FOXM1-FOXO1 axis. *Oncogene* 2022; **41**: 3778-3790 [PMID: 35761036 DOI: 10.1038/s41388-022-02394-8]

38 **McGettigan SE**, Debes GF. Immunoregulation by antibody secreting cells in inflammation, infection, and cancer. *Immunol Rev* 2021; **303**: 103-118 [PMID: 34145601 DOI: 10.1111/imr.12991]

39 **Tian Y**, Xiao H, Yang Y, Zhang P, Yuan J, Zhang W, Chen L, Fan Y, Zhang J, Cheng H, Deng T, Yang L, Wang W, Chen G, Wang P, Gong P, Niu X, Zhang X. Crosstalk between 5-methylcytosine and N(6)-methyladenosine machinery defines disease progression, therapeutic

response and pharmacogenomic landscape in hepatocellular carcinoma. *Mol Cancer* 2023; **22**: 5 [PMID: 36627693 DOI: 10.1186/s12943-022-01706-6]

40 **Sperandio RC**, Pestana RC, Miyamura BV, Kaseb AO. Hepatocellular Carcinoma Immunotherapy. *Annu Rev Med* 2022; **73**: 267-278 [PMID: 34606324 DOI: 10.1146/annurev-med-042220-021121]

41 **Boyault S**, Rickman DS, de Reyniès A, Balabaud C, Rebouissou S, Jeannot E, Hérault A, Saric J, Belghiti J, Franco D, Bioulac-Sage P, Laurent-Puig P, Zucman-Rossi J. Transcriptome classification of HCC is related to gene alterations and to new therapeutic targets. *Hepatology* 2007; **45**: 42-52 [PMID: 17187432 DOI: 10.1002/hep.21467]

42 **Liu M**, Jiang L, Guan XY. The genetic and epigenetic alterations in human hepatocellular carcinoma: a recent update. *Protein Cell* 2014; **5**: 673-691 [PMID: 24916440 DOI: 10.1007/s13238-014-0065-9]

43 **Ren F**, Li W, Xiang A, Wang L, Li M, Guo Y. Distribution and difference of APOBEC-induced mutations in the TpCpW context of HBV DNA between HCC and non-HCC. *J Med Virol* 2020; **92**: 53-61 [PMID: 31429946 DOI: 10.1002/jmv.25572]

44 **Long J**, Wang A, Bai Y, Lin J, Yang X, Wang D, Jiang Y, Zhao H. Development and validation of a TP53-associated immune prognostic model for hepatocellular carcinoma. *EBioMedicine* 2019; **42**: 363-374 [PMID: 30885723 DOI: 10.1016/j.ebiom.2019.03.022]

45 **Wang S**, Shi H, Liu T, Li M, Zhou S, Qiu X, Wang Z, Hu W, Guo W, Chen X, Guo H, Shi X, Shi J, Zang Y, Cao J, Wu L. Mutation profile and its correlation with clinicopathology in Chinese hepatocellular carcinoma patients. *Hepatobiliary Surg Nutr* 2021; **10**: 172-179 [PMID: 33898558 DOI: 10.21037/hbsn.2019.09.17]

46 **Pan Y**, Han M, Zhang X, He Y, Yuan C, Xiong Y, Li X, Zeng C, Lu K, Zhu H, Lu X, Liu Q, Liang H, Liao Z, Ding Z, Zhang Z, Chen X, Zhang W, Zhang B. Discoidin domain receptor 1 promotes hepatocellular carcinoma progression through modulation of SLC1A5 and the mTORC1 signaling pathway. *Cell Oncol (Dordr)* 2022; **45**: 163-178 [PMID: 35089546 DOI: 10.1007/s13402-022-00659-8]

47 **Cao F**, Luo A, Yang C. G6PD inhibits ferroptosis in hepatocellular carcinoma by targeting cytochrome P450 oxidoreductase. *Cell Signal* 2021; **87**: 110098 [PMID: 34325001 DOI: 10.1016/j.cellsig.2021.110098]

48 **Hu B**, Yang XB, Sang XT. Development and Verification of the Hypoxia-Related and Immune-Associated Prognosis Signature for Hepatocellular Carcinoma. *J Hepatocell Carcinoma* 2020; **7**: 315-330 [PMID: 33204664 DOI: 10.2147/JHC.S272109]

49 **Cai J**, Sun X, Guo H, Qu X, Huang H, Yu C, Wu H, Gao Y, Kong X, Xia Q. Non-metabolic role of UCK2 links EGFR-AKT pathway activation to metastasis enhancement in hepatocellular carcinoma. *Oncogenesis* 2020; **9**: 103 [PMID: 33277463 DOI: 10.1038/s41389-020-00287-7]

50 **Wu C**, Xia D, Wang D, Wang S, Sun Z, Xu B, Zhang D. TCOF1 coordinates oncogenic activation and rRNA production and promotes tumorigenesis in HCC. *Cancer Sci* 2022; **113**: 553-564 [PMID: 34904330 DOI: 10.1111/cas.15242]

51 **Liu J**, Zhang SQ, Chen J, Li ZB, Chen JX, Lu QQ, Han YS, Dai W, Xie C, Li JC. Identifying Prognostic Significance of RCL1 and Four-Gene Signature as Novel Potential Biomarkers in HCC Patients. *J Oncol* 2021; **2021**: 5574150 [PMID: 34257652 DOI: 10.1155/2021/5574150]

Published by **Baishideng Publishing Group Inc**
7041 Koll Center Parkway, Suite 160, Pleasanton, CA 94566, USA
Telephone: +1-925-3991568
E-mail: bpgoffice@wjgnet.com
Help Desk: https://www.f6publishing.com/helpdesk
https://www.wjgnet.com